Graz University of Technology

Master Thesis

# Robust Transit Time Measurement for Ultrasound Flowmeters

conducted at the
Signal Processing and Speech Communications Laboratory
Graz University of Technology, Austria

in co-operation with
AVL List GmbH
Graz, Austria

by
Michael Tauch, 0573083

Assessor:
Assoc.Prof. Dipl.-Ing. Dr. Klaus Witrisal

External Supervisor:
Dr. Katarzyna Kudlaty (AVL)

Graz, November 15, 2011

# Statutory Declaration

I declare that I have authored this thesis independently, that I have not used other than the declared sources/resources, and that I have explicitly marked all material which has been quoted either literally or by content from the used sources.

| | |
|---|---|
| date | (signature) |

# Abstract

Measuring the flow rate of a gas is an important task for the optimization of combustion engines. This work presents an adaptive signal processing method for ultrasound transit time flowmeters. An existing measurement system, developed by the AVL List GmbH, is investigated in terms of the transmission behavior of its transducers. Electrostatic (capacitive) ultrasound transducers have been developed by the AVL to be used in this system. As opposed to the formerly used piezo-electric transducers, it is now possible to use signals with high bandwidth ($\sim$ 100 kHz), making advanced signal processing techniques possible.

MLS system identification is used to model the transmission behavior of the electrostatic transducers. With this knowledge, the time-varying groupdelay of the transducers is estimated. This allows for separating the system group delay from the desired transit-times. Considering error propagation and theoretical performance bounds, an efficient method for the estimation of the flow velocity is found. This method improves accuracy, especially for the critical operating scenario of low flow velocities.

Empirical short- and long term results for zeroflow measurements, conducted with the proposed algorithm, are presented and discussed. The proposed algorithm fulfills the required accuracy.

# Zusammenfassung

Für die Optimierung von Verbrennungsmotoren ist die exakte Messung des Gas-Massenflusses wichtig. In dieser Arbeit wird ein adaptiver Signalverarbeitungsalgorithmus für die Durchflussmessung mittels Ultraschall (Transit Time Verfahren) vorgestellt. Ein von der AVL List GmbH entwickeltes Messgerät wurde hinsichtlich des Übertragungsverhaltens der verwendeten Ultraschall Wandler analysiert. Elektrostatische (kapazitive) Ultraschall Wandler wurden speziell für dieses Gerät von der AVL entwickelt. Im Gegensatz zu den früher verwendeten piezoelektrischen Wandlern sind jetzt hohe Signal Bandbreiten ($\sim 100$ kHz) realisierbar, was leistungsfähigere Techniken der Signalverarbeitung ermöglicht.

Um das Übertragungsverhalten der elektrostatischen Wandler zu modellieren wird eine MLS System Identifikation durchgeführt. Damit ist es möglich die zeitvariante Gruppenlaufzeit der Wandler von der gewünschten Messgröße zu trennen. Theoretische Überlegungen zur Fehlerfortpflanzung bilden die Grundlage für eine neue effizientere Berechnungsmethode der Strömungsgeschwindigkeit. Diese Methode verbessert die Messgenauigkeit speziell für den kritischen Fall niedriger Strömungsgeschwindigkeiten.

Empirische Ergebnisse für kurz- und langzeit Messungen des zero-flow Szenarios zeigen, dass die geforderte Genauigkeit erreicht wird.

**Acknowledgements**

This thesis would not have been possible without my supervisor Assoc.Prof. Dipl.-Ing. Dr. Klaus Witrisal who always provided me with guidance, support and expertise. I greatly appreciate having Univ.-Prof. Dipl.-Ing. Dr.techn. Gernot Kubin and Dipl.-Ing. Dr.techn. Markus Brandner in my examination committee.

I also want to thank the AVL and especially the project coordinator Katarzyna Kudlaty and Stefan Nöhammer, the indispensable hardware expert, for their support and help with the measurements.

A big hearty thanks goes out to my colleague Hannes, with whom I shared countless fruitful disscussions, likeminded collaboration, a great deal of diversion and nourishing lunch breaks.

I also would like to thank Brigitta, who gave me mental support, motivation and love, especially in the nerve-stretching final stage of writing.

I want to express my deepest gratitude towards my parents Gabriele and Wolfgang, who supported me throughout my studies, and without whom I would not be where I am today.

Last but not least, since this thesis concludes my years of study, I want to thank all teachers and colleagues that accompanied me along my way.

THANK YOU!

# Contents

# List of Figures

# 1 Introduction

*"Basic research is like shooting an arrow into the air and, where it lands, painting a target."*
*– Homer Burton Adkins*

## 1.1 Motivation

In recent years the optimization of combustion engines has made accurate gas-flow measurements very important. High gas temperatures, especially in the exhaust train, as well as rapidly varying flow velocities, demand a highly complex measurement routine. The *AVL List GmbH* has conducted extensive research in this field over the past years, resulting in a measurement device which is designed to operate both in the intake and exhaust gas train. While there are many different possibilities to measure the gas flow velocity within a pipe, the AVL decided to implement the ultrasound transit-time method. This method uses two opposing ultrasound transducers which measure the time it takes an ultrasound pulse to travel from one side of the measurement pipe to the other, to estimate the flow velocity within the pipe. The piezo-electric ultrasound transducers which were

used in earlier approaches were replaced by electrostatic transducers specifically developed for this task. This killed two birds with one stone, namely the strong limitations of piezo-electronic transducers regarding the operable temperature range as well as their very limited bandwidth. Another big advantage of electrostatic transducers is their great impedance matching for coupling soundwaves into air, i.e. less energy is lost during transmission from the mechanical domain of the membrane into the acoustical domain of the transmitting medium. The development of these broadband and heat resistant transducers however lead to new challenges. Neither a reliable system model to describe the behavior of the transducers under certain conditions, nor the respective signal processing methods which could exploit the high bandwidth exist. Apart from that it was observed, that the transmission behavior of the transducers was not stable over time. With further research, knowledge has been gained in both areas. To justify this new measurement technique (besides its applicability for high temperatures) a respectively high measurement accuracy is required. Preliminary work explored the physics and fluid dynamics of gas within a pipe, required pulse repetition frequencies, the effects of temperature gradients and non-uniform flow- or pressure profiles along the pipe, different algorithmic approaches as well as different sensor positions and mounting methods.[1, Wiesinger],[2, Kupnik]

### 1.1.1 Aim of this Thesis

The aim of this thesis is to tailor an adaptive signal processing algorithm to the existing measurement hardware, which can cope with the varying response characteristics of the transducers, and thus make robust transit time estimation possible. As prerequisite for this task, a model for the system at hand has to be found. System identification is performed on the transmission behavior of the electrostatic transducers. Reciprocity and error propagation as well as theoretical performance bounds are considered. With the information gained, a measurement routine is developed which uses both coherent phase and magnitude information. The proposed algorithm has been tested under different conditions and shown to meet the accuracy requirements.

### 1.1.2 Outline

This thesis is divided into three main parts. The introduction establishes the basics of flow measurement and explains fundamental aspects of the transit time flowmeter.

In Chapter 2 the theoretical concepts behind system identification with maximum length sequences are covered, followed by a detailed description of the methods used to build the proposed algorithm. This includes the fitting of bandpass models, group delay calculations, error propagation and theoretical performance bounds. Chapter 2 finishes

with a summary of the proposed algorithm.

The third part (Chapter 3) discusses the empirical results and relates the performance of the proposed method to the accuracy requirements.

## 1.2 Flow Measurement

The following sections describe the basics of flow measurement in Section 1.2.1, followed by a detailed description of the transit time flowmeter in Section 1.2.2. A short discussion on robustness and stability issues (Section 1.2.3) rounds off the first part of this introductory chapter.

### 1.2.1 Basic Principles

Flow measurement is a technique used in almost every industry that has to deal with gases or liquids. When talking about flow measurement the desired measurement quantity is usually the flowrate inside a pipe during a certain time $\left[\frac{kg}{h}\right]$. The direct measurement of mass however is often impossible (consider non-invasively measuring the mass of gas within a pipe). Fortunately the measurement of the flow velocity in $\left[\frac{m}{s}\right]$ is often easier and can also be related to the massflow, if geometric conditions as well as mass densities are known. In the case of measuring gases, this implies knowledge of the current temperature, the composition of the gas and the current pressure. The innumerable areas of application led to an equally innumerable amount of different measurement techniques. It is beyond the scope of this work to give an overview over all the current flowmeter techniques. Instead the focus will be set on a class of flowmeters called transit time flowmeters. Theses flowmeters are usually designed using ultrasound sensors. Not all ultrasound flowmeters are transit time flowmeters, for instance there are also so called Doppler flowmeters. A good overview of ultrasound flowmeters is given in [3, Lynnworth] and [4, Jacobsen]. The next section will explain the functionality of a transit time flowmeter in detail.

### 1.2.2 Transit Time Flowmeter (TTF)

A transit time flowmeter uses at least two different time measures (usually called upstream and downstream transit time). These quantities describe the time it takes a signal (e.g. an ultrasound pulse) to travel from one side of the measurement pipe to another, where upstream indicates the signalpath against the flow stream and downstream accordingly along the signalpath down the stream. The measurement of the upstream and downstream transit times can be either performed unidirectional, i.e. using two signal paths with two

opposing sensors each, or bidirectional, i.e. using only one signal path. However, the mathematical representation is the same regardless of the setup. If a bidirectional setup is used, then both sensors act as transmitter and receiver respectively. First, the signal is transmitted simultaneously from both sensors (transmission mode). In the time it takes the signals to travel to the opposing sensor, the operating mode is switched to receiving mode. Tab. 1.1 shows different properties of the two methods.

| **Unidirectional** | **Bidirectional** |
|---|---|
| - more hardware required | - less hardware required |
| - arbitrarily long signals possible | - length of transmission signal is restricted to minimal time of flight |
| - different systems for upstream and downstream | - same system for upstream and downstream |
| - crosstalk unavoidable | - no crosstalk between receiving channels |

*Table 1.1: Unidirectional vs. bidirectional flow measurement setup*

The bidirectional setup was used for this work, but all described techniques and principles can be applied to the unidirectional setup as well. Fig. 1.1 shows the basic set up of a bidirectional TTF. The left figure relates to the actual physical setup, whereas the right figure gives the equivalent system description for one direction (upstream or downstream respectively). The soundpath between the two transceivers TC1 and TC2 is modeled as pure delay and the receivers as Nth order bandpass respectively.. With $c$ being the sound

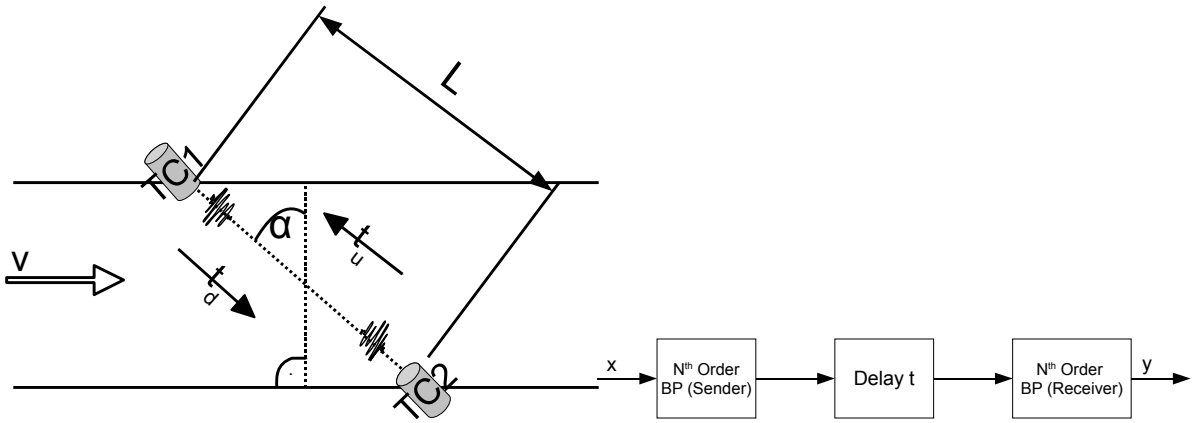


(a) physical description system (b) theoretical description

*Figure 1.1: System description of a transit time flowmeter*

velocity of the medium between the transceivers, L the distance between membranes of

TC1 and TC2 and $\alpha$ the angle between the normal axis and the sound path, the equations for the upstream transit time $t_u$ and the downstream transit time $t_d$ can be calculated as follows

$$\frac{L}{t_u} = c - v \cdot \sin\alpha$$
$$\frac{L}{t_d} = c + v \cdot \sin\alpha$$
$$t_u = \frac{L}{c - v \cdot \sin\alpha} \tag{1.1}$$
$$t_d = \frac{L}{c + v \cdot \sin\alpha} \tag{1.2}$$

If both $t_u$ and $t_d$ are solved for $c$ and combined the flow velocity is given by

$$v = \frac{L}{2 \cdot \sin\alpha} \cdot \frac{t_u - t_d}{t_u \cdot t_d} \tag{1.3}$$

Correspondingly, if solved for $v$, the actual sound velocity $c$ along the sound propagation path can be calculated

$$c = \frac{L}{2} \cdot \frac{t_u + t_d}{t_u \cdot t_d} \tag{1.4}$$

Strictly speaking, as shown in [2, Kupnik], (1.3) and especially (1.4) only hold true if the following very strong assumptions are made:

- The velocity profile across the measuring pipe is constant, i.e. there are no turbulences, including the transducer cavities
- The temperature along the sound propagation path is constant
- The is no sound drift, i.e. the transmitted pulse is not 'blown away' by the gas flow

Unfortunately these assumptions are quite a step away from reality. There exist various extensions and amendments to (1.3) and (1.4) which are also discussed in [2, Kupnik]. The algorithm developed in this work can however apply to these more sophisticated equations as well.

The detailed description of how the values of $t_u$ and $t_d$ are measured is presented in Section 2.2

### 1.2.3 Parameter Drift and Robustness Issues

A key point of interest in dealing with any system is to find an appropriate description of the behavior of the system under different circumstances. If a system changes its

characteristics over time, there are two possibilities to cope with this problem. Either one tries to find a better system model that makes the variations deterministic, or an adaptive algorithm is designed to compensate for the variation of the system parameters. While the first approach is clearly 'better' in terms of understanding a system, the latter does not require as much specific information on the system. Since a complete and accurate description of the system *transit time flowmeter* is very complex, this work implements the latter approach, i.e. the development of a robust algorithm for transit time estimation. There are many factors which can influence the robustness of this algorithm. The main influence, the time varying transducer characteristics, are covered within the proposed algorithm. However the investigation of the reasons why the characteristics of the transducers are time variant are beyond the scope of this work. In the following, a few contributions that investigate into this area, are presented.

The physical conditions inside a measuring pipe and their contributions to flowmetering have been explored in [5, Lysak et al.] and [6, Lysak et al.]. The authors present a stochastic model of turbulence as well as its application to flowmeters.

Apparent non-reciprocity in ultrasound flowmeters is discussed in [7, Deventer et al.]. The authors investigate the effects of manufacturing variations of piezo-electronic transducers. Their main observation is that even very small variations in parameters like piezo-electric disc thickness and permeability have a huge effect on the reciprocity of a transducer system. Even though they investigated piezo-electric transducers their results can be applied to electrostatic transducers as well. E.g, that drift in zero-flow measurement can only be prevented by proper calibration of non-identical sensors.

[8, Caronti et al.] try to formulate an accurate model for capacitive ultrasonic transducers in terms of equivalent electronic circuits.

The implications of pulsating flow and the corresponding measurement errors are investigated in [9, Berrebi et al.]. The authors propose a model for pulsations in flows including harmonics. With the resulting fundamental pulsation period they are able to improve measurement errors, that are related to a pulsating flow.

# 2

# Theory and Methods

*"The researches of many commentators have already thrown much darkness on this subject, and it is probable that, if they continue, we shall soon know nothing at all about it"*
*– Mark Twain*

This chapter consists of three parts. Section 2.1 describes the mathematical techniques that are required for system identification with maximum length sequences, as well as the fitting process of a bandpass model. The core of this work lies in Section 2.2 where the mathematical methods for robust transit time estimation are explained, along with performance considerations. Section 2.4 gives an algorithmic overview over the proposed method.

## 2.1 System Identification

This section describes the process of system identification with maximum length sequences (MLS). Section 2.1.1 explains how to generate maximum length sequences and the resulting important properties. The application of MLS on system identification is shown in Section 2.1.2. The process of fitting a bandpass model to a given impulse response is explained in Section 2.1.3. Finally Section 2.1.4 describes how to separate the transfer functions of two concatenated bandpass systems.

### 2.1.1 MLS Theory

Pseudo random noise sequences are a popular tool for system identification. Maximum length sequences (also called $m$-sequences or simply MLS), have some very special properties which will be discussed in the following. An $m$-sequence $m \in \{-1, 1\}$ of order $M$ is of length $L = 2^M - 1$. So a third-order $m$-sequence would be of length $2^3 - 1 = 7$. The $m$-sequence has a flat spectrum, apart from a small DC value ($\approx \frac{1}{L}$) which decreases with increasing order, and a crest factor of $c = 1$, which sets it apart from other pseudo random sequences that tend to have higher crest factors (for Gaussian noise $c \approx 4$). A low crest factor is important to properly excite the system which is to be measured, i.e. to bring a lot of energy into the system. To generate an $m$-sequence, a primitive binary polynomial of the same order is required. The task of finding primitive polynomials of higher orders is not trivial but has been studied by mathematicians. The theory behind this concept is beyond the scope of this work so we will rely on given primitive polynomials to generate $m$-sequences. Additional information about the use of $m$-sequences can be found here [10, Chu],[11, Ning]. For example, there exist two primitive binary polynomials $P1, P2$ of order $M = 3$: $P1 = 1 + x + x^3$ and $P2 = 1 + x^2 + x^3$. The respective binary coefficients $k_n \in 0, 1$ with $n = 0, 1...M$ and $k_0 = k_M = 1$ are $[1, 1, 0, 1]$, and$[1, 0, 1, 1]$. Either of these polynomials can be used in an $M$-stage linear feedback shift register to generate an $m$-sequence as follows:

$$\hat{m}_{i+1} = \sum_{n=0}^{M} k_n \hat{m}_{i-k} \mod 2 \tag{2.1}$$

where the mod operator takes the remainder of the division between its elements. This modulo operation is in general realized in hardware by using XOR elements. In the beginning each element in the register can be set to a random initial state. A different initial state will only result in a phase shift in the output sequence. The output sequence is periodic with length $L$. The conversion of the output sequence $\hat{m}$ with its binary description to the desired form $m \in \{-1, 1\}$, is simply obtained by calculating $m_i = 1 - 2\hat{m}_i$.

An important property of an $m$-sequence is that its cyclic auto-correlation is very similar to the Kronecker delta function $\delta[n]$. For non-zero lags the auto-correlation of the $m$-sequence is constant with the value $\frac{-1}{L}$, so for higher orders, the auto-correlation approaches the Kronecker delta function. Fig. 2.1 illustrates an $m$-sequence with $M = 3$ on the left and an $m$-sequence with $M = 6$ on the right, as well as their Fourier transforms and autocorrelations. The first frequency bin, i.e. the bin corresponding to te DC value, decreases with higher orders. Also the 'DC' offset in the auto-correlation decreases with increasing order. These properties result in a very effective calculation of the impulse response of the system, which is shown below.

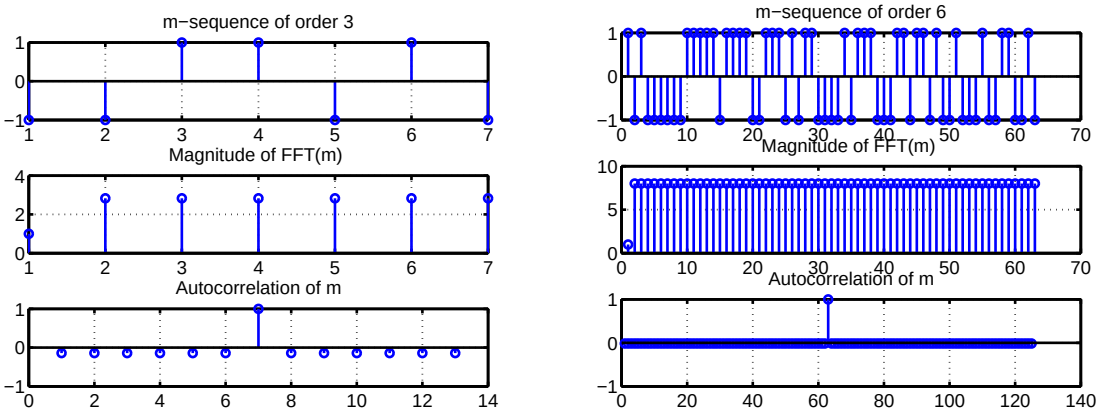


(a) 3rd-order $m$-sequence (b) 6th-order $m$-sequence

*Figure 2.1: Properties of m-sequences of different order*

## 2.1.2 System Identification with MLS

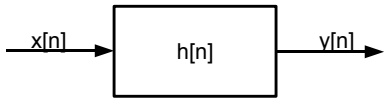


*Figure 2.2: A Standard LTI System*

An LTI system is shown in Fig. 2.2. It is completely characterized by its impulse response $h[n]$. If an input sequence $x[n]$ of length $N$ is applied to the system, the output $y[n]$ is given by

$$y[n] = x[n] * h[n] = \sum_{m=-\infty}^{\infty} x[m] \cdot h[n-m] \tag{2.2}$$

where the $*$ denotes convolution. Let $r_{ab}[k]$ denote the correlation sequence

$$r_{ab}[k] = \sum_n a[n] \cdot b[n+k] \tag{2.3}$$

So $r_{xx}[k]$ is the auto-correlation of the input sequence and $r_{xy}[k]$ the cross-correlation between input and output. An important property of LTI systems relates the cross-correlation of input and output with the autocorrelation of the input and the impulse response as follows

$$r_{xy}[k] = h[k] * r_{xx}[k] \tag{2.4}$$

The auto-correlation of an $m$-sequence with length $L$ is given by [11]

$$r_{xx}[k] = \frac{L+1}{L}\delta[k] - \frac{1}{L} \approx \delta[k] \text{ for } L >> 0 \tag{2.5}$$

If an $m$-sequence is used as input sequence $h[n]$ can now be determined conveniently as follows (using (2.4) and (2.5))

$$h[k] = r_{xy}[k] * \delta[k] = r_{xy}[k] \tag{2.6}$$

So by applying the cross-correlation between input and output, one immediately gets the impulse response. Time domain windowing can be used to separate noise and signal components in the impulse response, if necessary. Let

$$\bar{h}[n] = h[n] \cdot w[n] \tag{2.7}$$

denote the windowed impulse response, where $w[n]$ can be any window function. This work uses a half-sided *Tukey Window*, also known as *tapered cosine window*. It has the property of being flat in the beginning with a cosine roll-off towards the edge. Fig. 2.3 shows the original impulse response $h[n]$, as well as $\bar{h}[n]$ and the window function $w[n]$. The right hand side of Fig. 2.3 shows the effect of time-domain windowing on the frequency response. For better display,normalization of the sequences was performed both in the time and frequency domain. It is clearly convenient for further processing to use the smoothed frequency response.

For reduced computational complexity the cross-correlation, necessary to perform system identification, can also be replaced by the *Fast Hadamard Transform*, which works similar to the *Fast Fourier Transform* algorithm. This procedure is explained thoroughly in [10, Chu] and [11]. The following section describes how to fit a bandpass model to a identified system.

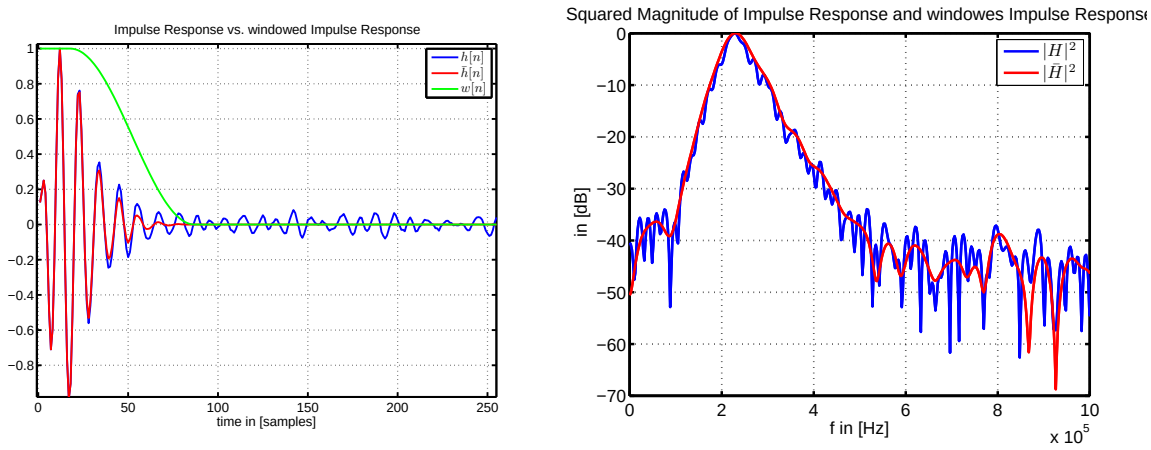


(a) Impulse Response (b) Squared Magnitude Response

*Figure 2.3: Effect of windowing on impulse response and frequency response*

### 2.1.3 Bandpass Model Fitting

Prior studies, e.g. [2, Kupnik], have shown, that electrostatic ultrasound transceivers have bandpass characteristics. A bandpass can be efficiently characterized by the following parameters: bandwidth, center frequency and roll-off factor. The bandwidth is defined as the passband region between the lower and the upper 3 dB cutoff frequencies. The roll-off factor describes how steep the edges of the filter are and depends on the filter order.

#### System Parameters

This section describes how to determine the 3 dB cutoff frequencies of a given bandpass system. Once obtained, they can be used to express useful system parameters, as the bandwith or the center frequency. From a given impulse response $h[n]$, e.g. as result of system identification with MLS, the complex frequency response $H[k]$ is computed via the Discrete-Fourier-Transform (DFT) as follows

$$H[k] = \sum_{n=0}^{N-1} h[n] \cdot \mathrm{e}^{-j2\pi \frac{k}{N} n} \tag{2.8}$$

where $k \in K$, where $K = \{0, 1, \ldots, N-1\}$ is the frequency bin index corresponding to $[0, f_s)$ with the resolution of $\frac{f_s}{N}$ and $N$ is the length of DFT. In the following $H_{dB}[k] = 20 \cdot \log(|H[k]|)$ corresponds to the squared magnitude response, given in dB, and is symmetric around $k = \frac{N}{2}$. For a DFT of size $N = 512$ and a sampling frequency $f_s = 2.5MHz$ this means that roughly 5 kHz are represented by one single frequency bin. To determine the 3 dB cutoff frequencies following approach has been chosen.

1. Find $k_M = \arg\max_k H_{dB}[k]$ and $H_{max} = H_{dB}[k_M]$.

2. Compute $\tilde{H}_{dB}[k] = H_{dB}[k] - H_{max} + 3dB$.

3. Compute $H_s[k] = \mathrm{sgn}(\tilde{H}_{dB}[k])$.

4. Find $k_L = \min(k_s)$ and $k_H = \max(k_s)$, where $\{k_s \in K \mid H_s[k_s] = 1\}$.

5. These two values $k_L$ and $k_H$ correspond to the frequency bins that are closest to the *true* 3 dB cutoff frequencies $f_L$ and $f_H$ (the subscripts $L$ and $H$ corresponding to the lower and upper 3 dB cutoff frequencies respectively).

6. Use linear interpolation to fit polynomials $P_L(f)$ and $P_H(f)$ through the two points $\left\{\tilde{H}_{dB}[k_L], \tilde{H}_{dB}[k_L - 1]\right\}$ and $\left\{\tilde{H}_{dB}[k_H], \tilde{H}_{dB}[k_H + 1]\right\}$, respectively.

7. Compute $f_L$ and $f_H$, where $P_L(f_L) = 0$ and $P_H(f_H) = 0$.

8. The resulting values correspond to the desired 'exact' values for $f_L$ and $f_H$.

Fig. 2.4 illustrates this process. Starting from the measured frequency response $H_{dB}[k]$, Steps 1 and 2 are performed to get $\tilde{H}_{dB}[k]$ (blue line). Step 3 computes the signum function $H_s[k]$ (red). Step 4 finds the minima $k_L$ and $k_H$. Once determined, only a linear interpolation is left to be done (step 5 to 8) . With $f_L$ and $f_H$ being known (green and magenta) the bandwidth is $B = f_H - f_L$ and the center frequency $f_C = \sqrt{f_L \cdot f_H}$. .

### Butterworth Fit

For a certain order and given pair of $f_L$ and $f_H$, a bandpass filter can be designed that matches this specification. There is a huge variety of filter types (Butterworth, Chebyshev, Elliptic ...) and design methods, each with different qualities such as passband ripple, stopband ripple or side-lobe attenuation. One standard filter type is the *Butterworth-Filter*, named after its inventor. It is specified to have a maximally flat frequency response in the passband (no ripple), as well as a roll-off towards zero in the stopband. Once the cut-off frequencies are known, there are a lot of different possibilities to design a filter. In this work the following technique (taken from the MATLAB Signal Processing Toolbox) was used.

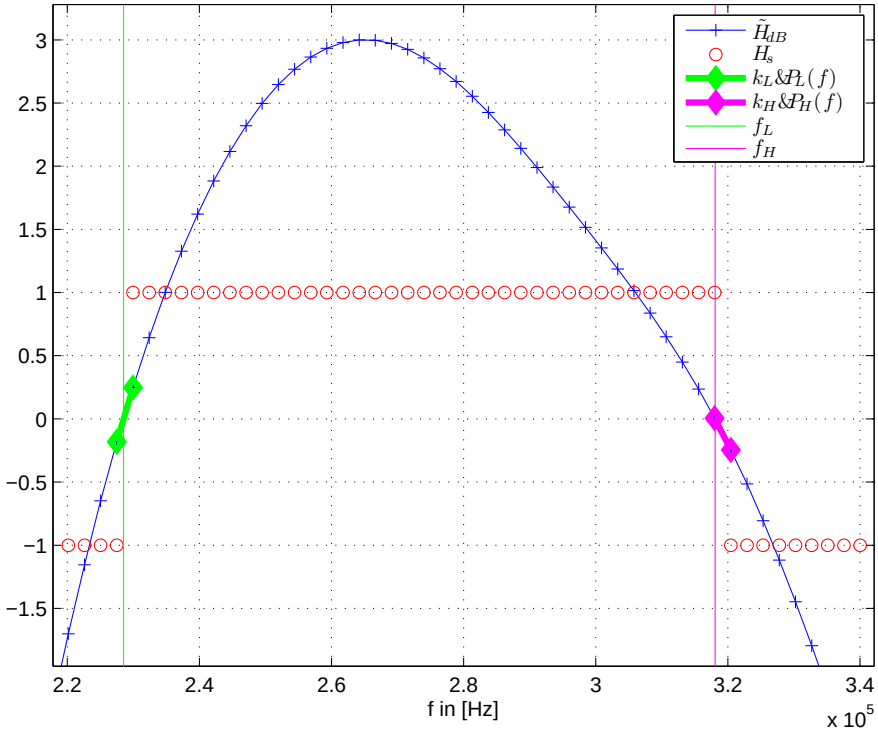


*Figure 2.4: Estimation of 3 dB cut-off frequencies*

1. Determine the lowpass analog prototype filter.

2. Convert poles and zeros in state-space form.

3. Transform lowpass prototype into bandpass to match cut-off frequencies using state-space transformation.

4. Convert from analog filter to digital filter with the bilinear transform.

5. Convert from state-space form to frequency response form.

The process of filter design is extensively covered in [12, Oppenheim]. Once the filter model has been determined, all interesting characteristics, such as impulse response, frequency response, phase response, group delay response etc... can be computed.

Fig. 2.5 shows the result of a system identification (Section 2.1.2) with subsequent parameter estimation and Butterworth model fitting. The left hand side displays the

measured windowed impulse response $\bar{h}[n]$ along with the modeled impulse response $\bar{h}_f[n]$ (where the subscript $f$ stands for *fit*). The model impulse response has been windowed with the same window $w[n]$ as in (2.7), to facilitate group delay and phase computations. The right hand side shows the according magnitude responses. The model magnitude response $|\bar{H}_f|^2$ has the same pass band and roll-off characteristics as the measured response $|\bar{H}|^2$ but without the noise floor at $\sim -40$dB.

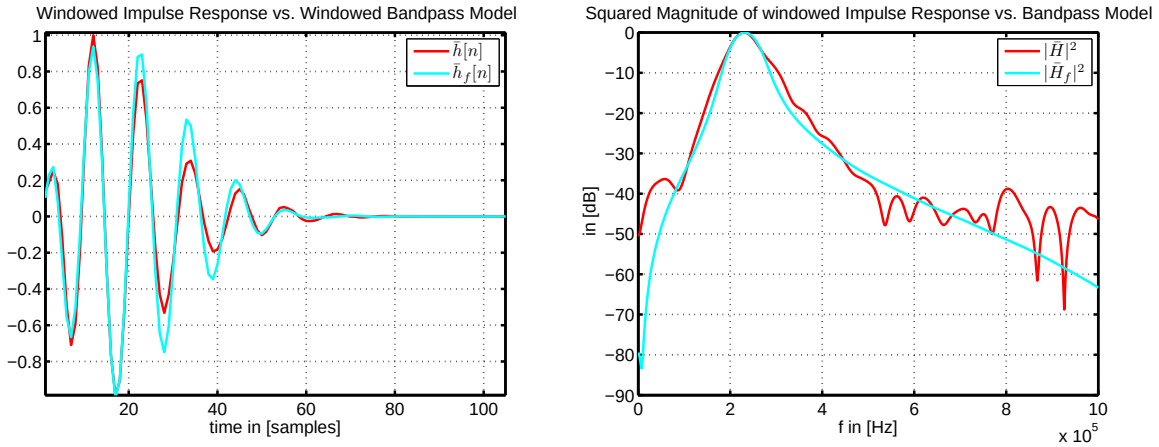


(a) Impulse response

(b) Squared magnitude response

*Figure 2.5: Measured system vs. bandpass model*

### Least Squares Fit

The system that has to be identified consists of two bandpass systems (Fig. 2.6). Each of these systems has a unique structure, independent from each other. For instance, the two systems could have different gain factors. A Butterworth model can only account for the lower and upper cut-off frequency which heavily confines the filter model.

It is also possible to fit a filter to match a desired frequency response in the passband. There not only two frequency points are specified but arbitrarily many (depending on the frequency resolution). The filter model is tuned, such that the error between the frequency response of the filter and the desired frequency response is minimized in a least squares sense.

It turned out however that this technique often produced filters with instable poles. Having more degrees of freedom that the Butterworth approach it is also less robust. It is not used in the final algorithm and therefore not explained any further in this work.

### Reciprocity

As mentioned earlier, perfect reciprocity is a very strong assumption which does not hold in practise. With the estimated system parameters of the upstream and downstream

measurement, two very convenient measures for reciprocity can be defined.

1. The difference between the bandwidths of the upstream and downstream model:
   $\Delta_B = B_u - B_d$

2. The difference between the center frequencies of the upstream and downstream model:
   $\Delta_C = f_{C,u} - f_{C,d}$

3. The group delay of the division of upstream and downstream frequency responses:
   $\Delta_G = \mathcal{G}\{\frac{H_u}{H_d}\}$

$\mathcal{G}\{\cdot\}$ is the group delay (see Section 2.2.3). All measures are zero in the case of perfect reciprocity. If they grow, it shows that reciprocity does not hold anymore and that the flow velocity estimations are corrupted by bias. There is a very close relationship between $\Delta_G$ and $\Delta_B$. The are perfectly correlated but with different units. $\Delta_G$ is measured in seconds, whereas $\Delta_B$ is measured in Hertz.

In Section 3.3 the relationship between reciprocity and measurement accuracy are shown.

### 2.1.4 System Decomposition

If MLS system identification is applied to a system as shown in Fig. 1.1, the resulting transfer function consists of two individual transfer functions, one corresponding to each transducer. Therefore it is not possible to measure the acoustic transmission behavior of a single transducer directly. To separate the transfer functions of the two transducers from each other, the following approach was used. A modified version of this approach can be found in [13, Anderson]. With three measurements, where three transducers are used in a combinatoric fashion, it is possible to determine the individual systems. For the sake of simplicity let the complex transfer function

$$H(\mathrm{e}^{j\omega}) = |H(\mathrm{e}^{j\omega})| \cdot \mathrm{e}^{\angle H(\mathrm{e}^{j\omega})} \tag{2.9}$$

be denoted by $H$. Choosing a set of three transducers $T_a, T_b, T_c$, three bidirectional measurements, each using two out of the three transducers, are performed. This results in the complex transfer functions $H_{a,b}, H_{a,c}, H_{b,c}$ from the upstream and $H_{b,a}, H_{c,a}, H_{c,b}$ from the downstream respectively, where the subscripts $H_{i,j} = H_i \cdot H_j$ denote that the transducer $T_i$ acts as the sender and $T_j$ as the receiver. Assuming reciprocity, that is

$H_{i,j} = H_{j,i} \,\forall\, (i,j) \in \{a,b,c\}$, it follows that

$$(H_a)^2 = \frac{H_{a,b} \cdot H_{a,c}}{H_{b,c}} = \frac{H_{b,a} \cdot H_{c,a}}{H_{c,b}}$$
$$(H_b)^2 = \frac{H_{b,a} \cdot H_{b,c}}{H_{a,c}} = \frac{H_{a,b} \cdot H_{c,b}}{H_{c,a}}$$
$$(H_a)^2 = \frac{H_{c,a} \cdot H_{c,b}}{H_{a,b}} = \frac{H_{a,c} \cdot H_{a,b}}{H_{b,a}}$$

and taking the square root (using equation (2.9))

$$H_a = \sqrt{\frac{H_{a,b} \cdot H_{a,c}}{H_{b,c}}} = \sqrt{\frac{|H_{a,b}| \cdot |H_{a,c}|}{|H_{b,c}|}} \cdot \mathrm{e}^{j\frac{1}{2}\angle\frac{H_{a,b}\cdot H_{a,c}}{H_{b,c}}} = \sqrt{\left|\frac{H_{a,b} \cdot H_{a,c}}{H_{b,c}}\right|} \cdot \mathrm{e}^{j\frac{1}{2}\angle H_{a,b}+\angle H_{a,c}-\angle H_{b,c}}$$
$$H_b = \sqrt{\left|\frac{H_{b,a} \cdot H_{b,c}}{H_{a,c}}\right|} \cdot \mathrm{e}^{j\frac{1}{2}\angle H_{b,a}+\angle H_{b,c}-\angle H_{a,c}}$$
$$H_c = \sqrt{\left|\frac{H_{c,a} \cdot H_{c,b}}{H_{a,b}}\right|} \cdot \mathrm{e}^{j\frac{1}{2}\angle H_{c,a}+\angle H_{c,b}-\angle H_{a,b}}$$

Results of the system identification are shown in Section 3.2

## 2.2 Transit-Time Estimation

This section describes the proposed algorithm to get a robust estimate for the transit times. Up to now only the 'raw' transit time $\tilde{t}$, including the group delay of the sending and receiving transceiver, has been measured. The contribution of the transceivers is normally regarded as constant, which enables calibration to eliminate their effects. However, since their transmission behavior is neither time invariant nor deterministic with respect to changing operating conditions (see Section 1.2.3), the key problem is to constantly determine estimates of their group delays. Fig. 2.6 shows the structure of the system behind this task. The *true* time of the airborn signal (without the additional group delays) is named $t$ here and will be later referred to as $t_u$ and $t_d$ for the upstream and downstream respectively. Since both transceivers are of the same type it can be safely assumed, that they can be represented by bandpasses of the same order $N$. An equivalent but more convenient structure is shown on the right hand side of Fig. 2.6. Here only one bandpass of order $2N$ accounts for both group delays introduced by the two transceivers. This makes the model fitting more convenient (see Section 2.1.3).

The first step is to determin the time it takes the signal to travel through the complete system. This procedure is explained in detail in Section 2.2.1. Section 2.2.2 describes the essential method to robustly estimate the beginning of the impulse responses of the upstream and downstream systems. Section 2.2.3 then describes the estimation of the group delays so that they can be separated from the overall system delay..

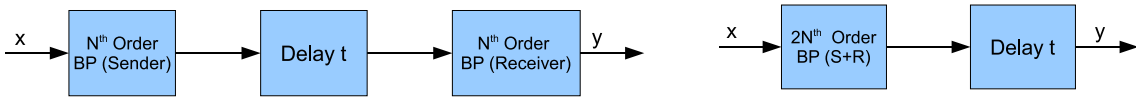


(a) overall system (b) equivalent description

*Figure 2.6: System model for a transit time flow meter*

## 2.2.1 Crosscorrelation

The general idea behind a TTF has already been laid out in Section 1.2.2. The method of choice to determine the delay between a signal $x[n]$ and a time-shifted version $y[n] = x[n-\tau]$ is the cross-correlation $r_{xy}[k]$. For infinitely long discrete signals, it is defined as:

$$r_{xx}[k] = \sum_{k=-\infty}^{\infty} x[n] \cdot y[n+k] \tag{2.10}$$

This is essentially the same as a convolution. The only difference is that the second sequence is not time reversed. $r_{xy}[n]$ has a maximum for $k = \tau$, so by finding the maximum one automatically determines the desired time-shift. If the system through which $x[n]$ is sent would consist of a pure delay, i.e. its impulse response would be all zero except for one unity pulse $\delta[n-\tau]$, this would be all one has to do to get $t$. However, the impulse response of a system like Fig. 2.6 is a theoretically infinitely long decaying sequence. Thus $y[n]$ is not merely a time-shifted version of $x[n]$. Instead $y[n] = h[n] * x[n]$ where $h$ is the impulse response and the '$*$' denotes convolution. The position of the maximum of $r_{xx}[k]$ is now also influenced by the group delay of the bandpass characteristics of the transducers.

If the transducers are regarded to be linear systems, then the overall measured delay between $x[n]$ and $y[n]$ is the sum of airborn flight time $t$ and the group delay of the transducers $\tau_G$, because $y[n] = h[n] * x[n-\tau]$. Fig. 2.7 and Fig. 2.8 show the two cases discussed above. As input signal a gaussian noise burst of length 100 samples has been chosen. In the first case $h[n]$ was a pure delay of 150 samples. The peak of the cross

correlation in Fig. 2.7 occurs exactly at 150 samples, corresponding to the correct delay $t = \tau = 150$.

As second example, a 4th-order Butterworth bandpass was designed using the 'fdatool' of MATLAB to simulate a transducer system. $h[n]$ consists now of a decaying impulse response, which starts at an offset of 150 samples. In Fig. 2.8 the maximum of the cross correlation is at $k = 152$, due to the group delay induced by the system.

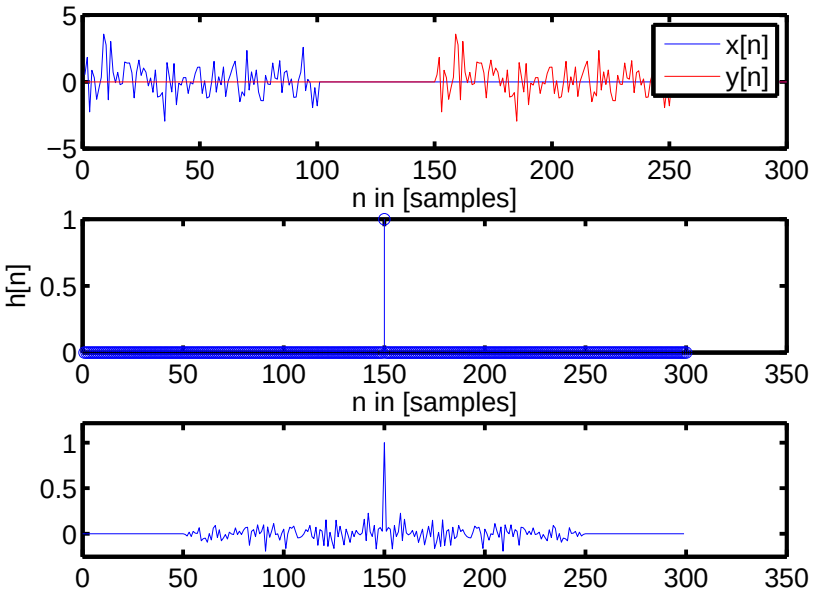


*Figure 2.7: $x[n], y[n], h[n]$ and $r_{xy}[k]$ for a pure delay*

If the input sequence is an m-sequence, then the crosscorrelation with the output sequence is the impulse response of the system $h[n]$ (Recall Section 2.1.2).

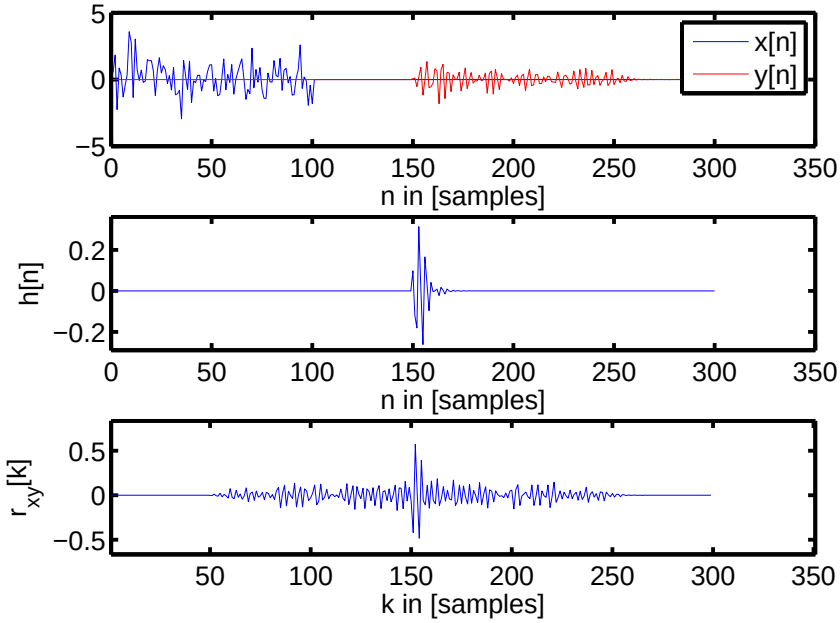


*Figure 2.8: $x[n], y[n], h[n]$ and $r_{xy}[k]$ for a 4th-order bandpass system*

### 2.2.2 Robust Transit Time Estimation

In general the starting point of an impulse response is hard to determine, when measurement noise is present. In the scenario of transit time estimation it is however vital to determine the exact time of the beginning of the impulse response. An accuracy of a fraction of a sample is required. After convolution of the MLS with the output sequence, a window has to be applied to cut the relevant portion of the impulse response out of the cross-correlation sequence. Fig. 2.9 shows the process of finding the starting point of such a window.

1. Compute the envelope $\tilde{h}[n] = |h[n] + j \cdot \mathcal{H}\{h[n]\}|$ , where $\mathcal{H}\{\cdot\}$ denotes the Hilbert transformation,[12, Oppenheim].

2. Find $n_m = \arg\max_n \tilde{h}[n]$

3. Find the integer starting index $n_s = n_m - n_o$

$n_o$ stands for a fixed offset which was empirically chosen to be 10 samples. $n_m$ does not mark the exact maximum of the envelop, but only the sample closest to the maximum. The starting index $n_s$ corresponds to the transit time in seconds via $\tilde{t} = n_s/fs$. This is of

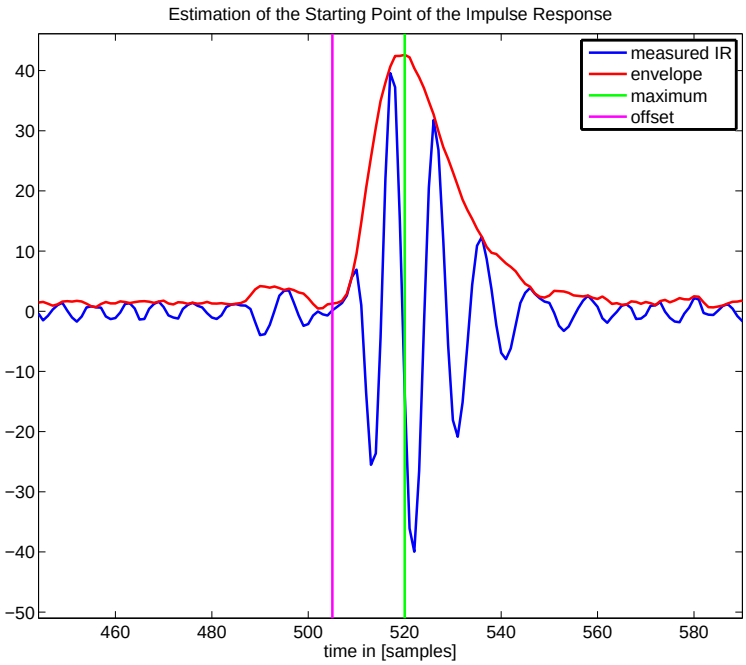


*Figure 2.9: Estimation of the starting point of a measured impulse response*

course not the true transit time, but with the group delay estimation techniques described in Section 2.2.3, the fractional delay between model and measurement can be calculated.

To demonstrate that this approach is valid, following simulation was performed. For different offsets $10 \leq n_o \leq 14$ the impulse response of the measured system was determined. An offset does not change the magnitude response but only the phase response and thus the group delay. Therefore the cut-off frequencies remain unchanged, which results in the same Butterworth model, regardless of the chosen offset.

However an offset of one sample leads to an additional constant group delay of 1 sample. The calculated difference between measured and modeled group delay changes accordingly. This makes estimation of the correct starting time very robust.

Fig. 2.10 shows the measured group delay for different offsets (blue), along with the modeled group delay (black). The different measured group delays differ by the amount of one sample from each other, whereas the group delay of the bandpass model remains unchanged. This proves that the proposed method is valid.

The next step is to separate the additional group delay of the transducers from the measured transit time.

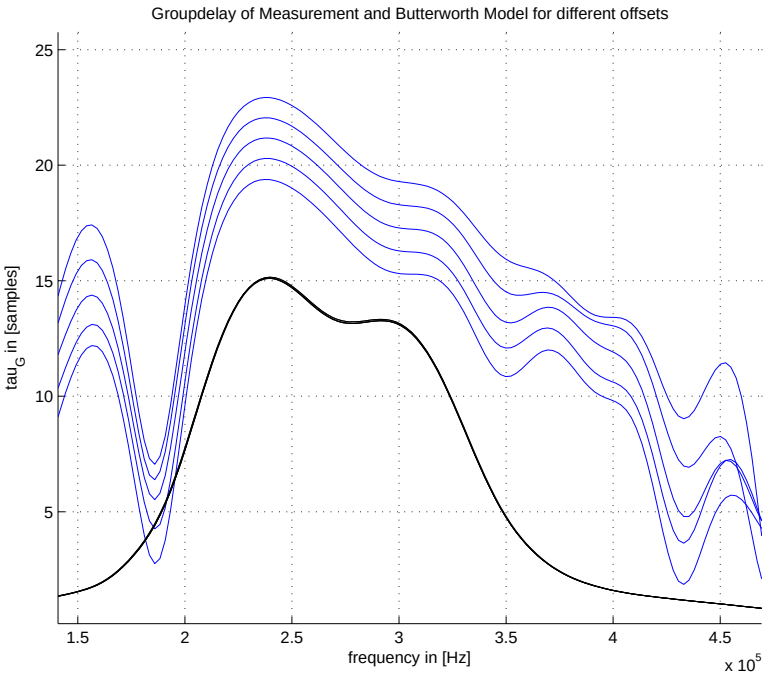


*Figure 2.10: Group delay of measurement and butterworth model for different offsets*

### 2.2.3 Group Delay Estimation

The group delay of a system with complex frequency response $H(\mathrm{e}^{j\omega})$ is defined as the negative gradient of the phase response

$$\tau(\omega) = -\frac{d\phi(\omega)}{d\omega} = -\frac{d\left(\arg\ H(\mathrm{e}^{j\omega})\right)}{d\omega} \tag{2.11}$$

For a discrete system $H[k], \quad k = \{0, 1, \ldots, N-1\}$, with $\phi[k] = \arg(H[k])$, the differentiation is reduced to a simple difference calculation

$$\tau[k] = -\frac{\phi[k] - \phi[k-1]}{k - (k-1)} = -(\phi[k] - \phi[k-1]) \tag{2.12}$$

If $\phi[k]$ is defined in [rad], this corresponds to a group delay in [rad], so $\tau[k]$ has to be divided by $\frac{2\pi N}{f_s}$ to get the group delay in [s].

Together with the information gained from the band pass model fitting (Section 2.1.3), there are several possibilities to accomplish the separation of the transducer group delays and the desired transit time.

### Linear Phase Approximation

The simplest and most robust way is to compute the slope of the measured phase response directly, by fitting a straight line to the passband section of the phase response. There are two points needed for this procedure. Convenient for further calculations are the $3dB$ cut-off frequencies $f_L$ and $f_H$ calculated as shown in Section 2.1.3 and already known from the band pass model fitting.

The slope of a line $y = m \cdot x + c$ is simply computed by

$$\frac{dy}{dx} = \frac{\Delta_y}{\Delta_x} = \frac{y(x_2) - y(x_1)}{x_2 - x_1} = m \tag{2.13}$$

The measured phase is of course not linear, so fitting a straight line to the passband section of the phase is only an approximation. Let $\phi(f)$ be the phase value at frequency $f$, then

$$\Delta_\phi = \phi(f_H) - \phi(f_L), \quad \Delta_f = f_H - f_L \tag{2.14}$$

and the average group delay of the measurement in the passband $\overline{\tau_M}$ becomes

$$\overline{\tau_M} = -\frac{d\phi}{df} \approx -\frac{\Delta_\phi}{\Delta_f} \tag{2.15}$$

It is known from filter theory, that the phase response of a 2N-th order bandpass drops by $N \cdot \frac{\pi}{2}$. With this, the reference group delay $\tau_L$ becomes

$$\tau_L = -\frac{N \cdot \frac{\pi}{2}}{\Delta_f} = -\frac{N\pi}{2\Delta_f} \tag{2.16}$$

Together with the transit times $\tilde{t}$ determined via cross-correlation (Section 2.2.1) this yields

$$t_L = \tilde{t} - (\overline{\tau_M} - \tau_L) = \tilde{t} + \frac{\Delta_\phi}{\Delta_f} - \frac{N\pi}{2\Delta_f} = \tilde{t} + \frac{2\Delta\phi - N\pi}{2\Delta_f} \tag{2.17}$$

where the subscript $L$ stands for the linear approximation method.

On the upside this method is computationally efficient and very robust. On the downside the approximation of the phase response with a straight line can be rather coarse, depending on the system parameters of the individual transducers (i.e. for not identical systems).

In Fig. 2.11 the measured phase response (blue) as well as the reference line (magenta) are shown for a 4th order bandpass system.

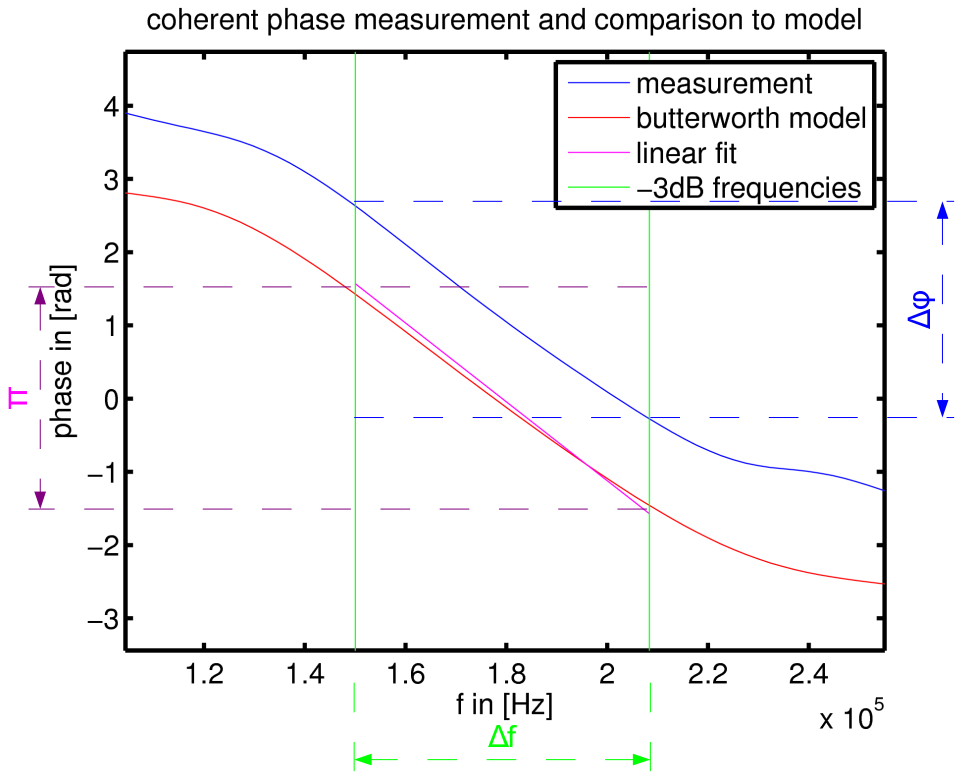


*Figure 2.11: Coherent phase measurement and comparison to 4th order model*

### Butterworth Approximation

If a Butterworth filter was designed with the parameters extracted from the measured impulse response, the group delays of the measurement and the model can be subtracted directly. Fig. 2.11 shows the measured phase response (blue) as well as the phase response of the Butterworth model (red). The slope of the two graphs is almost identical. Let $\tau_M$ denote the group delay of the measured impulse response and $\tau_B$ the group delay of the Butterworth fit (both calculated via (2.12)). Together with the transit time $\tilde{t}$ this yields

$$t_B = \tilde{t} - \frac{1}{k_H - k_L} \sum_{k=k_L}^{k_H} \tau_M[k] - \tau_B[k] \tag{2.18}$$

where the subscript in $t_B$ stands for the Butterworth approximation. In (2.18) the group delay difference within the passband $k_H - k_L$ is averaged.

## 2.3 Error Model and Performance Considerations

In this section an error model for the estimation of the stream velocity is introduced, followed by a discussion on error propagation and performance bounds.

### 2.3.1 Error Model

In a first step it is necessary to introduce a model for the measurement errors that occur. Let $\theta$ denote the measurement parameter. Assuming that the random error is normally distributed with variance $\sigma_\theta^2$ and mean $\mu_\theta$, the estimated value $\hat{\theta}$ of the true parameter value $\theta$ is defined as

$$\hat{\theta} \sim \mathcal{N}(\mu_\theta, \sigma_\theta^2), \quad f_{\hat{\theta}}(x) = \frac{1}{\sqrt{2\pi\sigma_\theta^2}} \cdot \mathrm{e}^{-\frac{(x-\mu_\theta)^2}{2\sigma_\theta^2}} \tag{2.19}$$

To describe the effect of an error on a measurement, the two terms accuracy and precision are often used. While accuracy relates to the bias $\theta - \mu_\theta$, precision usually refers to the standard deviation $\sigma_\theta$. When there is no error bias, then of course $\mu_\theta = \theta$, i.e. the estimation is perfectly accurate, or unbiased. Especially for the computation of error bounds, e.g. the Cramer-Rao bound (see Section 2.3.3), the estimators are restricted to be unbiased. If there is more than one parameter involved in the measurement, each parameter is distributed accordingly. For example if there are two parameters $\theta_1$ and $\theta_2$, and their according unbiased estimates $\hat{\theta}_1$ and $\hat{\theta}_2$ with the distributions $\hat{\theta}_1 \sim \mathcal{N}(\theta_1, \sigma_{\theta_1}^2)$ and $\hat{\theta}_2 \sim \mathcal{N}(\theta_2, \sigma_{\theta_2}^2)$ respectively, they are grouped for convenience in a parameter vector $\boldsymbol{\theta} = [\theta_1, \theta_2]^\mathrm{T}$ and an estimation vector $\hat{\boldsymbol{\theta}} = [\hat{\theta}_1, \hat{\theta}_2]^\mathrm{T}$

Whenever there is more than one parameter involved in a measurement, the individual errors do not have to be uncorrelated. A measure that describes the correlation between two random variables is the covariance, defined as

$$c_{1,2} = \mathrm{E}\Big\{(\hat{\theta}_1 - \mu_{\theta_1}) \cdot (\hat{\theta}_2 - \mu_{\theta_2})\Big\} \tag{2.20}$$

where $\mathrm{E}\{\cdot\}$ is the expectation operator. Computing $c_{1,1}$ is the variance $\sigma_{\theta_1}^2$. The covariance can also be expressed in terms of a correlation coefficient

$$r = \frac{c_{1,2}}{\sigma_1 \cdot \sigma_2}, \quad -1 \leq r \leq 1,\ r \in \mathbb{R}. \tag{2.21}$$

For an estimation vector $\hat{\boldsymbol{\theta}} = [\hat{\theta}_1, \hat{\theta}_2, \ldots, \hat{\theta}_M]^\mathrm{T}$ the corresponding variances and covariances can be conveniently written in an $[M \times M]$ covariance matrix.

$$\boldsymbol{C} = \begin{bmatrix} \sigma_{\hat{\theta}_1}^2 & c_{1,2} & \cdots & c_{1,M} \\ c_{2,1} & \sigma_{\hat{\theta}_2}^2 & \ddots & \vdots \\ \vdots & \ddots & \ddots & \vdots \\ c_{M,1} & \cdots & \cdots & \sigma_{\hat{\theta}_M}^2 \end{bmatrix} \tag{2.22}$$

with the symmetry property $c_{i,j} = c_{j,i} \quad i, j \in \{1, 2, \ldots, M\}$.

This error model is now applied to Equation (1.3). The are two different possibilities to compute the transit time difference in the numerator of (1.3). Either directly via cross-correlation of the received signals, or indirectly via the individual transit times.

Corresponding to the cross-correlation method, the desired quantity $v_1$ is a function of $t_u$,$t_d$ and $\Delta_t$.

$$v_1 = C \cdot \frac{\Delta_t}{t_u \cdot t_d} \tag{2.23}$$

If $\Delta_t$ is not measured directly, but computed via the individual measurements of $t_u$ and $t_d$ , then $v_2$ is only a function of $t_u$ and $t_d$ .

$$v_2 = C \cdot \frac{t_u - t_d}{t_u \cdot t_d} \tag{2.24}$$

where $C = L/(2 \cdot sin(\alpha))$, is the *geometric constant*.

The corresponding parameter vectors are

$$\boldsymbol{\theta_1} = [\Delta_t, t_u, t_d]^{\mathrm{T}} \tag{2.25}$$

and

$$\boldsymbol{\theta_2} = [t_u, t_d]^{\mathrm{T}} \tag{2.26}$$

In other words $v_1 = v_1(\boldsymbol{\theta_1})$, and $v_2 = v_2(\boldsymbol{\theta_2})$.

### 2.3.2 Covariance Transformation

The following approach is a standard method in statistics, e.g. [14, Kay].

Let $\hat{\boldsymbol{\theta}} = [\hat{\theta}_1, \hat{\theta}_2, \ldots, \hat{\theta}_M]^{\mathrm{T}}$ be the estimation vector, i.e. a set of estimated parameters. Provided that the covariance matrix of $\hat{\boldsymbol{\theta}}$ is known, the variance $\sigma_f^2$ of a function $f(\hat{\boldsymbol{\theta}})$ can be computed as

$$\sigma_f^2 = \boldsymbol{J_f}^{\mathrm{T}} \cdot \boldsymbol{C} \cdot \boldsymbol{J_f} \tag{2.27}$$

where $\boldsymbol{J_f}$ is the $[M \times 1]$ Jacobian matrix with all first order derivatives, defined as

$$\boldsymbol{J_f} = \boldsymbol{J}\left(f(\boldsymbol{\theta})\right) = \begin{bmatrix} \frac{\partial f}{\partial \theta_1} \\ \frac{\partial f}{\partial \theta_2} \\ \vdots \\ \frac{\partial f}{\partial \theta_M} \end{bmatrix} \tag{2.28}$$

and $\boldsymbol{C}$ is the covariance matrix as defined in Section 2.3.1. Applied to the two calculation methods of the flow velocity, $v_1(\boldsymbol{\theta_1})$ and $v_2(\boldsymbol{\theta_2})$, the respective covariance matrices become

$$\boldsymbol{C_1} = \begin{bmatrix} \sigma^2_{\Delta_t} & c_{tu,\Delta_t} & c_{td,\Delta_t} \\ c_{\Delta_t,tu} & \sigma^2_{tu} & c_{td,tu} \\ c_{\Delta_t,td} & c_{tu,td} & \sigma^2_{td} \end{bmatrix} \tag{2.29}$$

and

$$\boldsymbol{C_2} = \begin{bmatrix} \sigma^2_{tu} & c_{td,tu} \\ c_{tu,td} & \sigma^2_{td} \end{bmatrix}. \tag{2.30}$$

Using symmetry properties, with $c_{tu,\Delta_t} = c_{td,\Delta_t} = c_{\Delta_t,tu} = c_{\Delta_t,td} = c_\Delta$ and $c_{tu,td} = c_{td,tu} = c_t$, this simplifies to

$$\boldsymbol{C_1} = \begin{bmatrix} \sigma^2_{\Delta_t} & c_\Delta & c_\Delta \\ c_\Delta & \sigma^2_{tu} & c_t \\ c_\Delta & c_t & \sigma^2_{td} \end{bmatrix} \tag{2.31}$$

and

$$\boldsymbol{C_2} = \begin{bmatrix} \sigma^2_{tu} & c_t \\ c_t & \sigma^2_{td} \end{bmatrix}. \tag{2.32}$$

The Jacobian matrices for $v_1$ and $v_2$ are

$$\boldsymbol{J_1} = C \cdot \boldsymbol{J}\left(\frac{\Delta_t}{t_u t_d}\right) = C \cdot \begin{bmatrix} \frac{1}{t_u t_d} \\ -\frac{\Delta_t}{t_u t_d^2} \\ -\frac{\Delta_t}{t_u^2 t_d} \end{bmatrix} \tag{2.33}$$

and

$$\boldsymbol{J_2} = C \cdot \boldsymbol{J}\left(\frac{t_u - t_d}{t_u t_d}\right) = C \cdot \begin{bmatrix} -\frac{1}{t_d^2} \\ \frac{1}{t_u^2} \end{bmatrix} \tag{2.34}$$

Using (2.27), the variances for the two different methods of flow estimation can now be computed:

$$\sigma^2_{v1} = \boldsymbol{J_1}^{\mathrm{T}} \cdot \boldsymbol{C_1} \cdot \boldsymbol{J_1} \tag{2.35}$$

$$= C^2 \left( \frac{2\Delta_t^2 c_t}{t_u^3 t_d^3} - \frac{2\Delta_t c_\Delta}{t_u^3 t_d^2} - \frac{2\Delta_t c_\Delta}{t_u^2 t_d^3} + \frac{\sigma^2_\Delta}{t_u^2 t_d^2} + \frac{\Delta_t^2 \sigma^2_{tu}}{t_u^4 t_d^2} + \frac{\Delta_t^2 \sigma^2_{td}}{t_u^2 t_d^4} \right) \tag{2.36}$$

$$\sigma_{v2}^2 = \boldsymbol{J_2}^{\mathrm{T}} \cdot \boldsymbol{C_2} \cdot \boldsymbol{J_2} \tag{2.37}$$

$$= C^2 \left( -\frac{2c_t}{t_u^2 t_d^2} + \frac{\sigma_{tu}}{t_d^4} + \frac{\sigma_{td}}{t_u^4} \right) \tag{2.38}$$

It can be safely assumed that the upstream and downstream transit time can be measured with the same precision, i.e. $\sigma_{tu}^2 = \sigma_{td}^2 = \sigma_t^2$. Furthermore the correlation between the direct measurement of $\Delta_t$ and $t_u$ or $t_d$ is negligible, i.e. $c_\Delta \approx 0$. With $t_u^2 \approx t_d^2 \approx t_d \cdot t_u = t^2$ (valid for low flow velocities), it follows that

$$\sigma_{v1}^2 \approx C^2 \cdot \left( \frac{2\Delta_t^2 c_t}{t^6} + \frac{\sigma_\Delta^2}{t^4} + \frac{2\Delta_t^2 \sigma_t^2}{t^6} \right) \tag{2.39}$$

and

$$\sigma_{v2}^2 \approx C^2 \cdot \left( -\frac{2c_t}{t^4} + \frac{2\sigma_t^2}{t^4} \right) \tag{2.40}$$

The covariance $c_t$ between the two transit time measurements, can also be expressed in terms of the correlation r. With $c_t = r \cdot \sigma_t^2$, it follows that

$$\sigma_{v1}^2 = \frac{C^2}{t^2} \cdot \left( \frac{\Delta_t^2}{t^2} \cdot \frac{2\sigma_t^2}{t^2} \cdot (1+r) + \frac{\sigma_\Delta^2}{t^2} \right) \tag{2.41}$$

and

$$\sigma_{v2}^2 = \frac{C^2}{t^2} \cdot \frac{2\sigma_t^2}{t^2} \cdot (1-r). \tag{2.42}$$

Furthermore note, that the correlation reduces the overall estimation variance $\sigma_{v2}^2$ but increases $\sigma_{v1}^2$. It is assumed that the relative error of the transit time difference estimation $\frac{\sigma_{\Delta_t}}{t}$ is considerably smaller than the relative error of the transit time estimation itself $\frac{\sigma_t}{t}$. At this stage it becomes clear, that especially for small flow velocities, where $\Delta_t \ll t$, the first method is favorable, since the transit time estimation variance $\sigma_t^2$ is weighted by $\Delta_t^2/t^2$.

Fig. 2.12 shows the predicted standard deviations, i.e. the precisions, $\sigma_{v1}$ and $\sigma_{v2}$ for $\sigma_{\Delta_t} = 10ns$ and $\sigma_t = 100ns$ (@ $t \approx 425\mu s$) and different values for $r$. These values for $\sigma_{\Delta_t}$ and $\sigma_t$ are taken from experimental results in Section 3.3. As bench mark, the requested precision of 1% relative error of the flow velocity is plotted (blue). It can be seen that the estimation variances for $\hat{v}_2$ are constant over the complete flow velocity range, whereas the estimation variances for $\hat{v}_1$ are ascending with $v$. As stated above, especially at low flow velocities ($v < 5\frac{m}{s}$) only $\hat{v}_2$ is better than the required precision. And depending on the correlation factor, $\hat{v}_1$ is clearly advantageous up to very high flow velocities. The correlation of the errors in the estimation of $t_u$ and $t_d$ does heavily affect the precision of

$\hat{v}_2$ but only slightly the precision of $\hat{v}_1$.

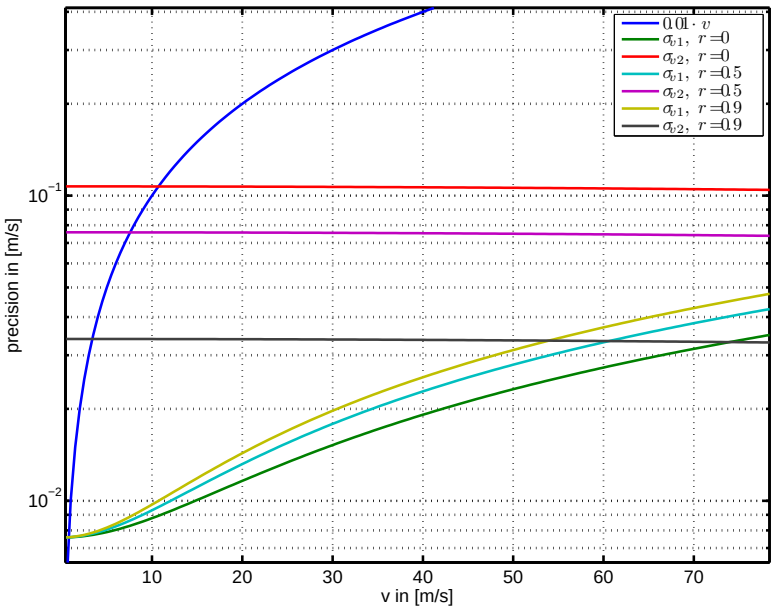


*Figure 2.12: Precision of different flow velocity estimates for $\sigma_{\Delta_t} = 10\,ns$ and $\sigma_t = 100\,ns$*

All the considerations that were made in this section imply that the estimation variances $\sigma^2_{\Delta_t}$ and $\sigma^2_t$ are known. If they are unknown, it is also possible to estimate a lower bound for the achievable estimation variances, based on a system and error model. The calculation of a popular error bound is described in the following section.

### 2.3.3 Cramer-Rao Lower Bound

The *Cramer-Rao Lower Bound* (CRLB) computes the optimum, i.e. lowest, achievable variance of an unbiased estimator. It is defined as the inverse Fisher-Information. The theory behind the determination of CRLBs as well as application examples are given in [14, Kay]. The author derives the CRLB for range estimation with radar, an example very similar to the task of transit time estimation. The following derivation is taken from [14, Kay].

The (continuous) signal model is given by

$$x(t) = s(t - \tau) + w(t) \tag{2.43}$$

where $x(t)$ is the received signal, $s(t)$ the transmitted signal and $w(t)$ white gaussian noise with PSD $\frac{N_0}{2}$. This is very similar to the computation of $\Delta_t$ since for perfect reciprocity the cross correlation between the received signals is essentially an correlation same signal

$s(t)$ where one is shifted by $\tau$. For this signal model, the Cramer Rao lower bound is given by

$$\mathrm{var}\{\hat{\tau}\} \geq \frac{\frac{N_0}{2}}{\int_0^T \left(\frac{ds(t)}{dt}\right)^2 dt}. \tag{2.44}$$

With the energy $E$,

$$E = \int_0^T s^2(t)dt \tag{2.45}$$

and the *mean squared bandwidth* $\bar{F^2}$,

$$\bar{F^2} = \frac{\int_0^T \left(\frac{ds(t)}{dt}\right)^2 dt}{\int_0^T s^2(t)dt} = \frac{\int_{-\infty}^{\infty} (2\pi f)^2 |S(f)|^2 df}{\int_{-\infty}^{\infty} |S(f)|^2 df} \tag{2.46}$$

(2.44) can be rewritten as

$$\mathrm{var}\{\hat{\tau}\} \geq \frac{1}{\frac{E}{N_0/2}\bar{F^2}} \tag{2.47}$$

The term $\frac{E}{N_0/2}$ is essentially an SNR. The mean squared bandwidth $\bar{F^2}$ is a normalized measure which includes bandwidth $B$ and center frequency $f_0$ of a bandpass signal $s(t)$. As an analytic approximation, the magnitude response of a bandpass can be modeled with a rectangular function as follows

$$|S_r(f)|^2 = \begin{cases} \frac{1}{2B}, & \text{for } \; f_0 - B/2 \leq |f| \leq f_0 + B/2 \\ 0, & \text{else} \end{cases}. \tag{2.48}$$

This definition ensures that

$$\int_{-\infty}^{\infty} |S_r(f)|^2 df = 1. \tag{2.49}$$

The mean square bandwidth of the rectangular magnitude response bandpass becomes

$$\bar{F_r^2} = \frac{\int_{-\infty}^{\infty} (2\pi f)^2 |S_r(f)|^2 df}{\int_{-\infty}^{\infty} |S_r(f)|^2 \, df} = \frac{2 \cdot \int_{f_0-B/2}^{f_0+B/2} (2\pi f)^2 \frac{1}{2B} \, df}{1}$$

$$= \frac{4\pi^2}{3B} f^3 \Big|_{f_0-B/2}^{f_0+B/2}$$

$$= 4\pi^2 f_0^2 + \frac{1}{3}\pi^2 B^2. \tag{2.50}$$

This clearly shows, that both $f_0$ and $B$ affect the performance of the estimation. However, the influence of the center frequency is much greater. With the quality factor

$$Q = \frac{f_0}{B} \tag{2.51}$$

(2.50) becomes

$$\bar{F_r^2} = 4\pi^2 f_0^2 + \frac{1}{3}\pi^2 \frac{f_0^2}{Q^2} = 4\pi^2 f_0^2 (1 + \frac{1}{12Q^2}) \approx 4\pi^2 f_0^2 \tag{2.52}$$

because it can be assumed that $Q > 2$.

Now with the rectangular frequency response approximation, and for given SNR and $f_0$ the resulting CRLB can be computed. Fig. 2.13 shows the achievable precision $\sigma_{\Delta_t}$ for different SNRs and center frequencies. It can be seen that changing the center frequency by one magnitude is equivalent to increasing the SNR by 20 dB. Both results in a change in $\sigma_{\Delta_t}$ by one magnitude.

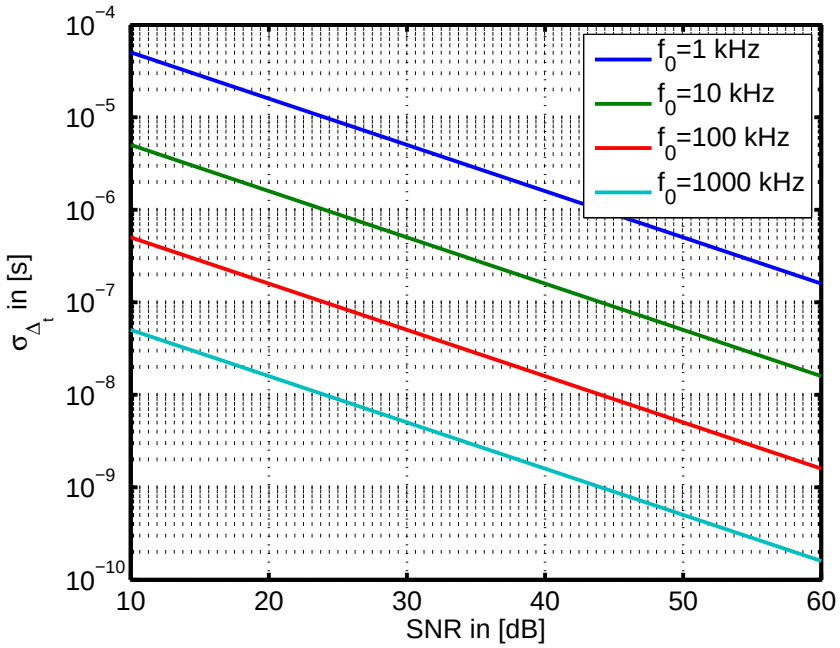


*Figure 2.13: CRLB of $\sigma_t$ for different SNR and $f_0$*

## 2.4 Algorithmic Overview

Fig. 2.14 shows a simplified overview of the proposed algorithm. Each time the flow velocity is to be estimated, the flow diagramm has to be run through once. Bold arrows resemble block processing, and thin arrows resemble scalar values. The two key improvements this algorithm provides, compared to other flow estimation methods are:

1. The time difference $\Delta_t$ is estimated directly via cross-correlation of the receiver signals, which allows for high measurement precision.

2. Due to the choice of $m$-sequences as input signal, a system identification is efficiently performed for upstream and downstream respectively, allowing for parameter drift compensation.

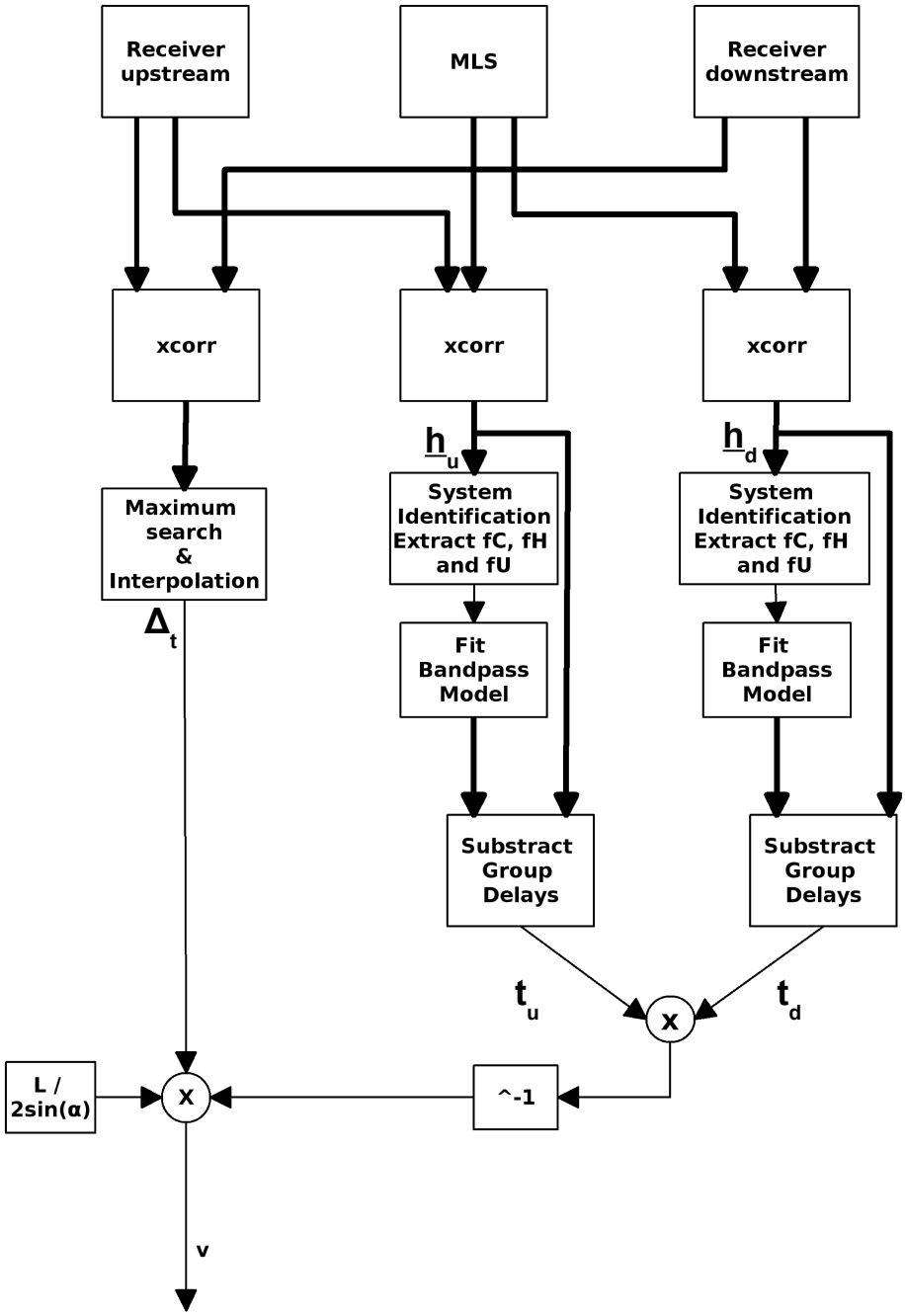


*Figure 2.14: Algorithmic overview*

The following enumeration summarizes the proposed algorithm and references the sections of this work, where the respective methods are explained.

1. Send the same $m$-sequence simultaneously upstream and downstream.

2. Perform cross-correlation between the received signals and m-sequence to get $h_u[k]$ and $h_d[k]$ (Section 2.1.2) and between the two received signals to get $\Delta_t$ (Section 2.2.1).

3. Find $n_s = \arg\max_n$ of the envelopes of the impulse responses $h_u$ and $h_d$ and substract the offset $n_o$, which yields the raw transit times $\tilde{t}_u[n]$ and $\tilde{t}_d[n]$ (Section 2.2.2).

4. For each system calculate the parameters $f_U$ and $f_H$ (Section 2.1.3).

5. Fit 4th-order Butterworth bandpass filters to match theses parameters (Section 2.1.3).

6. Compute the group delays of the filters ($\tau_{B,u}$ and $\tau_{B,d}$) and of the measured transfer functions from step 2 ($\tau_{M,u}$ and $\tau_{M,d}$) (Section 2.2.3)..

7. Compute the transit time estimates $\hat{t}_{B,u}$ and $\hat{t}_{B,d}$ (Section 2.2.3).

8. Use $\hat{t}_{B,u}$, $\hat{t}_{B,d}$ and $\hat{\Delta}_t$ to compute $v$ (Section 1.2.2).

# 3
# Results and Discussion

*"A couple of months in the laboratory can frequently save a couple of hours in the library"*
*– Westheimer's Law*

This chapter is divided into three sections. Section 3.1 describes the measurement setup used for the system identification as well as for the testing of the algorithm. Section 3.2 shows the results of the system identification for the electronic frontend and the transducers. In Section 3.3 the short and longterm measurement results for the proposed algorithm are presented.

## 3.1 Measurement Setup

Fig. 3.1 shows the measurement setup for system identification and algorithm testing. An *Agilent 33120A Arbitrary Waveform Generator* sends the $m$-sequences into the measurement hardware. The received signals are captured with a *LeCroy Ditigal Oscilloscope*. The analysis of the data is then performed in MATLAB after transferring the data to a

PC. The parameter settings, such as sampling frequency, MLS length and memory depth of the oscilloscope are described in the respective sections.

### 3.1.1 Setup for System Identification

The MLS system identification technique as described in Section 2.1 was applied to the transmitting and receiving electronics first (without the transducers). The transmitting electronics are essentially an inverting amplifier and a switch with an RC element, whereas the receiving electronics consist of an amplifier and a bandpass. A sampling frequency of 2 MHz and three periods of a 13th-order $m$-sequence were used ($3 \cdot 8191$ samples @ 2 MHz $\Rightarrow$ 12 ms). Each element of the signal chain was put under test separately.

In a second step, the transducers were connected. In contrast to the identification of the electronic front end, a maximum signal length of $\sim 100\,\mu s$ is possible. In the bidirectional setup the operating mode of the transceivers must be switched from transmitting to receiving (Section 1.2.2). To account for this restriction, 2 periods of an 8th-order $m$-sequence at a sampling frequency of 5 MHz were used ($2 \cdot 255$ samples @ 5 MHz $\Rightarrow$ $\sim 100\,\mu s$).

The setup in Fig. 3.1 shows that both, an upstream and a downstream frequency response can be computed, depending on the chosen receiver. The determination of the individual impulse responses of the transducers was performed according to Section 2.1.4.

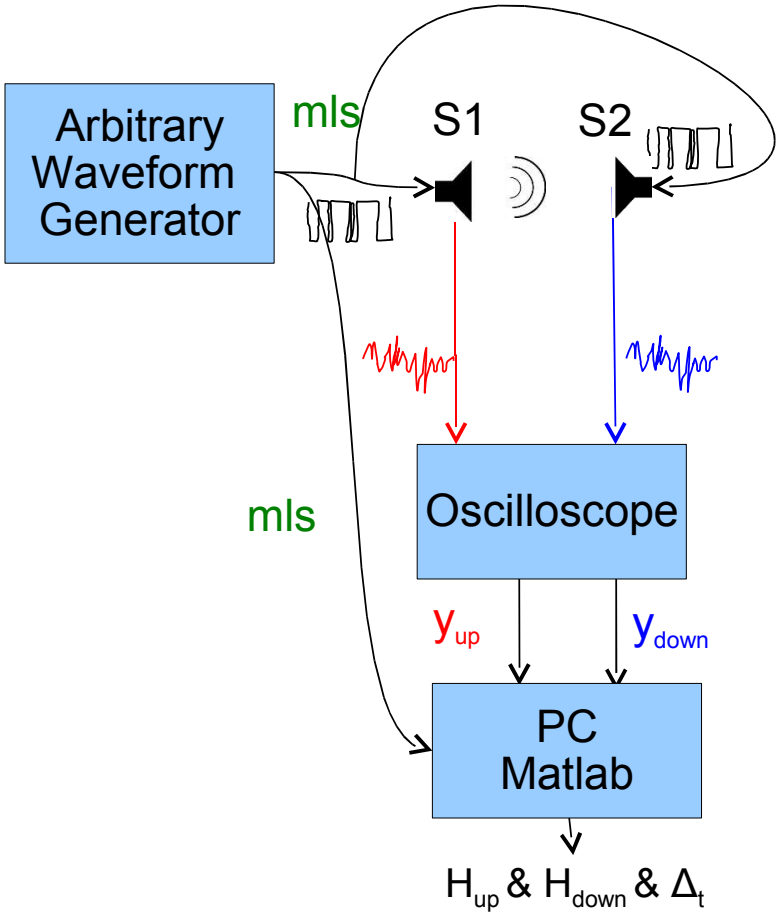


*Figure 3.1: Measurement setup for system identification and testing*

### 3.1.2 Setup for Algorithm Testing

The testing of the algorithm essentially uses the same setup as for the system identification of the transducers. The only difference is that the measurement routine is performed repeatedly. To facilitate the capture of measurement data following strategy was used.

In a real application scenario, the electronic hardware of the measurement device repeatedly generates pulses that trigger the transmission routine. The pulse repetition frequency is 1kHz. This trigger signal is fed into the signal generator, so that an $m$-sequence is sent every millisecond to the transducers. Due to the huge amount of data, the oscilloscope is not able to save all the received signals. So the trigger signal is also provided to the oscilloscope, where a hold-off value $N_h$ can be set. $N_h$ determines the number of trigger pulses the oscilloscope waits between automated savings of the received signals. So for every $N_h$-th trigger pulse, the oscilloscope saves the two receiving channels automatically. The formula for the required holdoff $N_h$ that results in a desired time resolution $t_{res}$ of the measurement is then

$$N_h = t_{res} \cdot 1000 \quad t_{res} \text{ in } [s] \tag{3.1}$$

So a hold-off value of $N_h = 10000$ corresponds to one measurement every 10 seconds. This method allows automated long term measurements, as performed in Section 3.3.2, with identical time intervals between the measurements.

The transducers are mounted in a measurement pipe with no flow applied, hence the term zero-flow measurement. The goal of this measurement is to observe the zero-stability of the flow velocity computation. To reduce polarization of the transducers, the bias voltage is typically switched every few seconds. For the measurements in Section 3.3 this switching is intentionally turned off to produce a parameter drift of the transducers.

## 3.2 System Identification

### 3.2.1 Electronic Frontend

Fig. 3.2 shows the results of the system identification of the transmitting electronics. The overall amplification is around 60 dB and the phase response matches the inverting characteristic of the amplifier. The abbreviations PA and RC stand for power amplifier and resistor-capacitor. As expected the RC element has zero amplification and phase. The reason why the sum of the two individual systems RC and PA is not equal to the measurement results of the complete system may be found in impedance matching of the measurement hardware.

Fig. 3.3 shows the results of the system identification of the receiving electronics. To avoid harmonics from the power supply scattering into the measurement, a galvanic separation between the measurement loop and the ground loop was performed using a transformer. The frequency and phase responses as shown in Fig. 3.3 are without calibration for the transformer characteristics, resulting in the drop off to high frequencies.

The results of the third measurement are shown in Fig. 3.4. Here the crosstalk between the two channels was measured. This is only important when a monodirectional setup is used, since only then a crosstalk can occur. The damping between transmitting and receiving electronics in the frequency range where the transducers operate is only between 20dB and 25dB. The reason for the discrepancy in the damping for the different crosstalk directions is not clear.

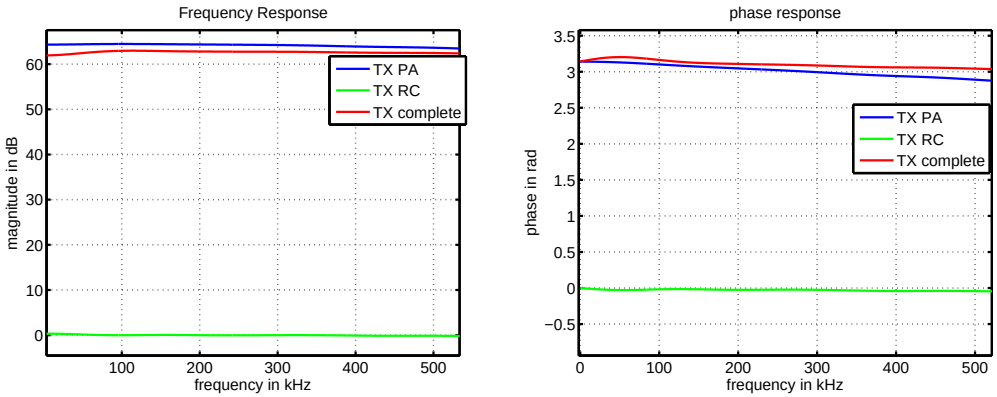


(a) Frequency Response (b) Phase Response

*Figure 3.2: System identification for transmitting electronics*

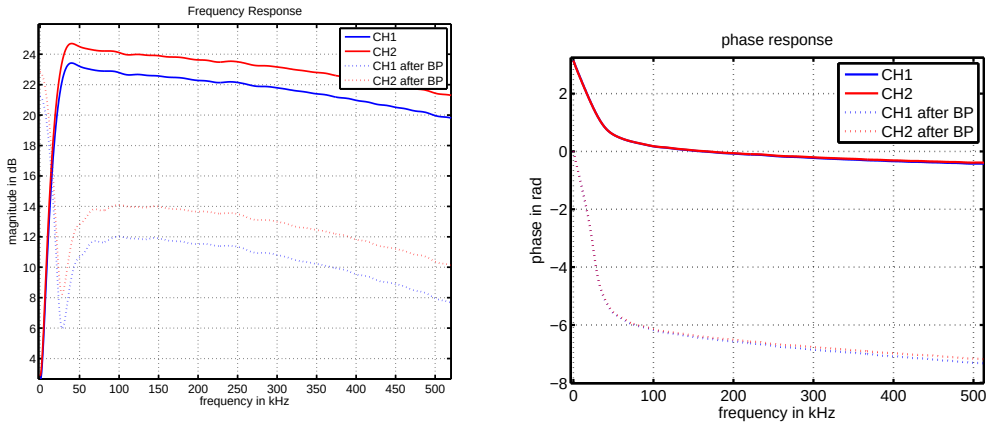


(a) Frequency response (b) Phase esponse

*Figure 3.3: System identification for receiving electronics*

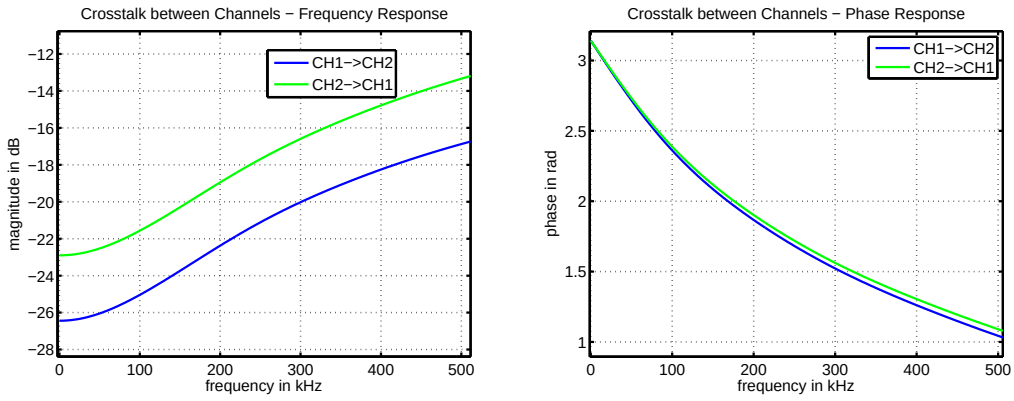


(a) Frequency response (b) Phase response

*Figure 3.4: System identification for crosstalk between channels*

### 3.2.2 Transducer Measurements

The system identification of the individual transducers was performed as shown in Section 2.1.4. It is known from filter theory, e.g. [15, Tietze, Schenk], that the phase response of a second order band pass spans an amount of $\pi$ over the whole frequency range and $\frac{\pi}{2}$ within the passband. Fig. 3.5 shows the frequency and phase response of six different transducers, as identified from the upstream measurements (see Section 2.1.4). The transducers T4, T5 and T9 are missing because they were damaged.

While having different center frequencies and bandwidths, the phase response clearly indicates that the bandpass system that describes a single transducer is of second order. This means that the concatenation of two transducers forms a band pass system of fourth order. This is a very important realization since it allows to model the transducer system as proposed in Section 2.1.3.

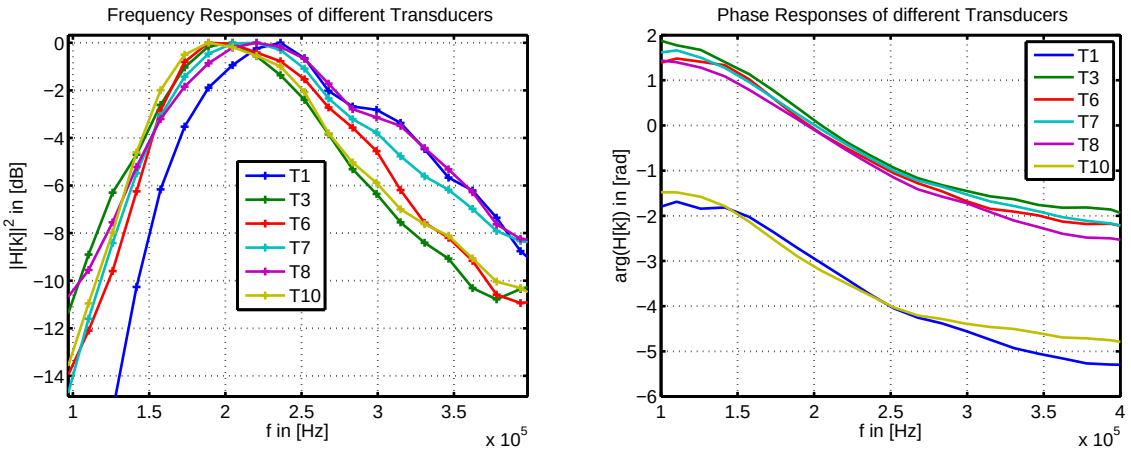


(a) Frequency response

(b) Phase response

*Figure 3.5: System identification for different transducers*

Fig. 3.6 shows the system identification results for the upstream (+) and the downstream (□) magnitude response. The figure on the left contains the results for the transducer triplet T1, T2 and T3. The figure on the right for the triplet T7, T8 and T10 respectively. The differences between upstream and downstream measurements in the passband are small, compared to the variations outside the passband, especially for transducers 3,6 and 8. This shows, that the assumption that a transducer can be treated as a reciprocal system is valid.

Fig. 3.7 gives an overview of the transducer characteristics as well as the differences for upstream and downstream decomposition ((2.9)). Transducers 1, 7 and 10 can be considered perfectly reciprocal, while the other transducers have a small mismatch between upstream and downstream response. The deviations among sensors are however clearly greater than the observed mismatch between upstream and downstream.

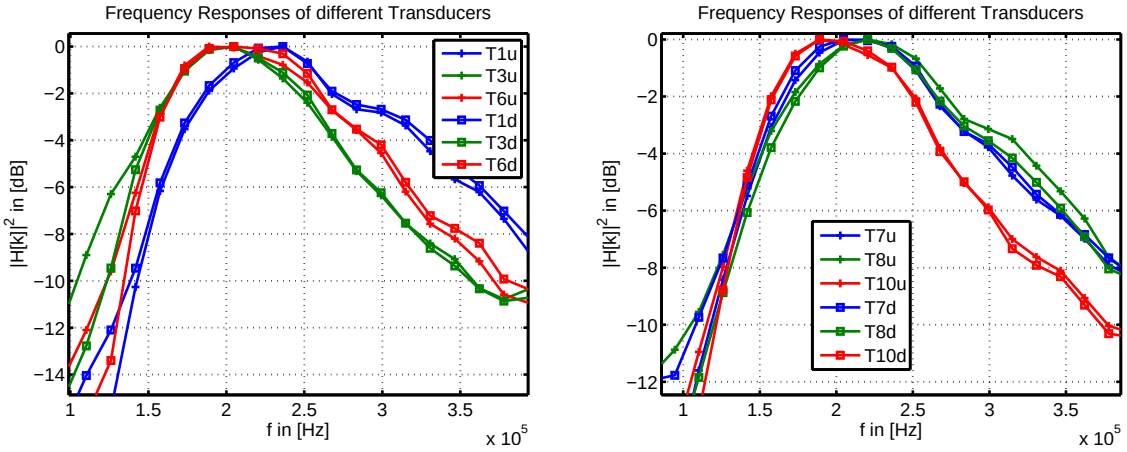


(a) Transducers 1 ,3 and 6 (b) Transducers 7, 8 and 10

*Figure 3.6: Comparison of upstream and downstream system identification of individual transducers*

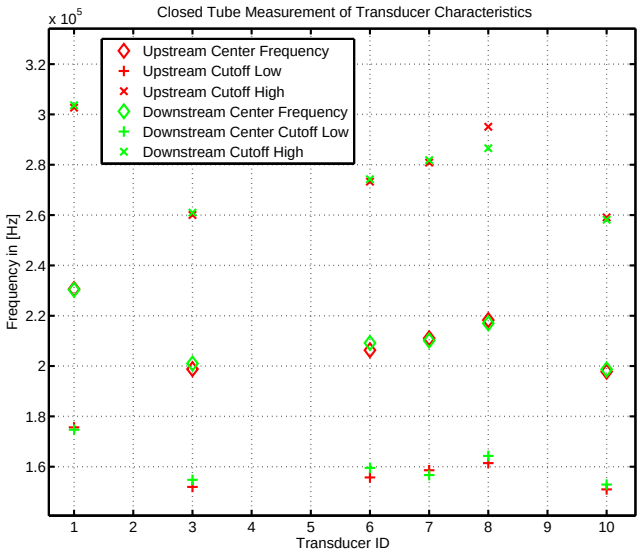


*Figure 3.7: Transducer parameters overview*

## 3.3 Zero Flow Measurements

A critical working scenario for a transit time flow meter is at low flow velocities. Therefore zero flow measurements were taken, to determine the stability and robustness of the transit time estimation.

### 3.3.1 Short Term Measurements

Five different sensor pairs were tested. Each pair was tested for 10 minutes, with 6 measurements per minute. The following tables show the standard deviation of different

parameter estimates. Each column corresponds to a sensor pair. In the last column the root mean square of all sensor pairs is computed. The estimated reference transit times $\hat{t}_{u,ref}$ and $\hat{t}_{d,ref}$ are calculated without group delay correction (only a fixed offset of 12 samples is subtracted from the interpolated peak of the estimated impulse responses).

Tab. 3.1 shows the standard deviations for the individual transit time estimates. The subscripts $L$ and $BW$ correspond to the linear fitting method and the Butterworth fitting method as described in Section 2.1.3. The linear fitting method only reduces the standard deviation of the estimated transit time by a factor of 2 compared to the estimated reference transit times. The Butterworth method reduces the standard deviation again by a factor of 2.

It is not clear why the standard deviation for the downstream transit time estimation is often considerably smaller than the upstream standard deviation. This effect may be related to an uncalibrated electronic frontend.

| | T1T2 | T3T4 | T5T6 | T7T8 | T9T10 | RMS |
|---|---|---|---|---|---|---|
| std of $\hat{t}_{u,ref}$ in [ns] | 262 | 357 | 358 | 251 | 358 | 321 |
| std of $\hat{t}_{d,ref}$ in [ns] | 279 | 220 | 350 | 318 | 353 | 308 |
| std of $\hat{t}_{u,L}$ in [ns] | 207 | 205 | 178 | 121 | 111 | 169 |
| std of $\hat{t}_{d,L}$ in [ns] | 180 | 165 | 93 | 127 | 111 | 139 |
| std of $\hat{t}_{u,BW}$ in [ns] | 70 | 78 | 70 | 85 | 68 | 74 |
| std of $\hat{t}_{d,BW}$ in [ns] | 76 | 66 | 56 | 61 | 67 | 66 |

*Table 3.1: Standard deviation of different transit time estimates*

Recalling Section 2.3.3, it plays an important role if the estimation errors are correlated. This can be seen in Tab. 3.2. It shows the precision of different estimates of the transit time difference, i.e. the numerator of (1.3). $\Delta_t$ is estimated directly via cross correlation of the received signals.

| | T1T2 | T3T4 | T5T6 | T7T8 | T9T10 | RMS | $\overline{r}$ |
|---|---|---|---|---|---|---|---|
| std of $\hat{t}_{u,ref} - \hat{t}_{d,ref}$ in [ns] | 384 | 414 | 460 | 396 | 463 | 425 | 0.14 |
| std of $\hat{t}_{u,L} - \hat{t}_{d,L}$ in [ns] | 55 | 37 | 64 | 63 | 46 | 54 | 0.86 |
| std of $\hat{t}_{u,BW} - \hat{t}_{d,BW}$ in [ns] | 36 | 32 | 50 | 60 | 40 | 45 | 0.84 |
| std of $\hat{\Delta}_t$ in [ns] | 5.4 | 5.6 | 7.6 | 5.7 | 3.5 | 5.7 | - |

*Table 3.2: Standard deviation of different estimates of the transit time difference*

$\hat{\Delta}_t$ is clearly the best estimator for the transit time difference. Compared to the reference method it achieves a standard deviation roughly two orders of magnitude smaller than the reference method. The linear fit already improves the estimation significantly and the Butterworth method outperforms the linear method. However both the linear and the Butterworth method are still one order of magnitude worse (in terms of standard deviation) than the direct estimation.

Comparing this results with the standard deviations of the individual transit times, it becomes clear that the errors of $\hat{t}_{u,ref}$ and $\hat{t}_{d,ref}$ have to be less correlated than the errors of $\hat{t}_{u,L}$ and $\hat{t}_{d,L}$, or $\hat{t}_{u,BW}$ and $\hat{t}_{d,BW}$ respectively. The averaged (over all five sensor pairs) correlation coefficient $\overline{r}$ between the two transit time estimates that are used in the respective row of Tab. 3.2, is shown in the last column. As shown in Section 2.3.3 a high correlation coefficient is favorable, since the errors cancel each other out in the difference computation. The advantage of using either of the model fitting methods becomes apparent when looking at the correlation factors. For $\hat{\Delta}_t$ no correlation factor can be determined, since it is measured directly. The correlation between the error of $\hat{\Delta}_t$ and any individual transit time estimate is however zero.

Tab. 3.3 shows 4 different flow velocity estimates, computed as follows

$$\hat{v}_{ref} = C \cdot \frac{\hat{t}_{u,ref} - \hat{t}_{d,ref}}{\hat{t}_{u,ref} \cdot \hat{t}_{d,ref}}, \tag{3.2}$$

$$\hat{v}_{L} = C \cdot \frac{\hat{t}_{u,L} - \hat{t}_{d,L}}{\hat{t}_{u,L} \cdot \hat{t}_{d,L}}, \tag{3.3}$$

$$\hat{v}_{BW} = C \cdot \frac{\hat{t}_{u,BW} - \hat{t}_{d,BW}}{\hat{t}_{u,BW} \cdot \hat{t}_{d,BW}}, \tag{3.4}$$

and

$$\hat{v}_{prop} = C \cdot \frac{\hat{\Delta}_t}{\hat{t}_{u,BW} \cdot \hat{t}_{d,BW}}. \tag{3.5}$$

| | T1T2 | T3T4 | T5T6 | T7T8 | T9T10 | RMS |
|---|---|---|---|---|---|---|
| std of $\hat{v}_{ref}$ in [cm/s] | 15.5 | 16.7 | 18.5 | 16 | 18.7 | 17.1 |
| std of $\hat{v}_{L}$ in [cm/s] | 2.1 | 2.5 | 3.4 | 3.2 | 3.5 | 3 |
| std of $\hat{v}_{BW}$ in [cm/s] | 1.7 | 2.2 | 2.4 | 2.9 | 3.4 | 2.6 |
| std of $\hat{v}_{prop}$ in [cm/s] | 0.22 | 0.23 | 0.31 | 0.23 | 0.14 | 0.23 |

*Table 3.3: Standard deviation of different flow velocity estimates*

The proposed method clearly outperforms the reference estimation. With an average of

$2.3\frac{mm}{s}$, $\hat{v}_{prop}$ is one order of magnitude better than the two methods $\hat{v}_L$ and $\hat{v}_{BW}$ which used the conventional method to calculate $v$. Even though $\hat{v}_L$ is much more efficient to compute (no butterworth bandpass model fitting is necessary), the standard deviation of its estimation error is almost equal to $\hat{v}_{BW}$.

Fig. 3.8 shows the estimated zero flow velocities $\hat{v}_{prop}$ for the different transducer pairs, corresponding to Tab. 3.3. There are positive and negative biases for the different trans-

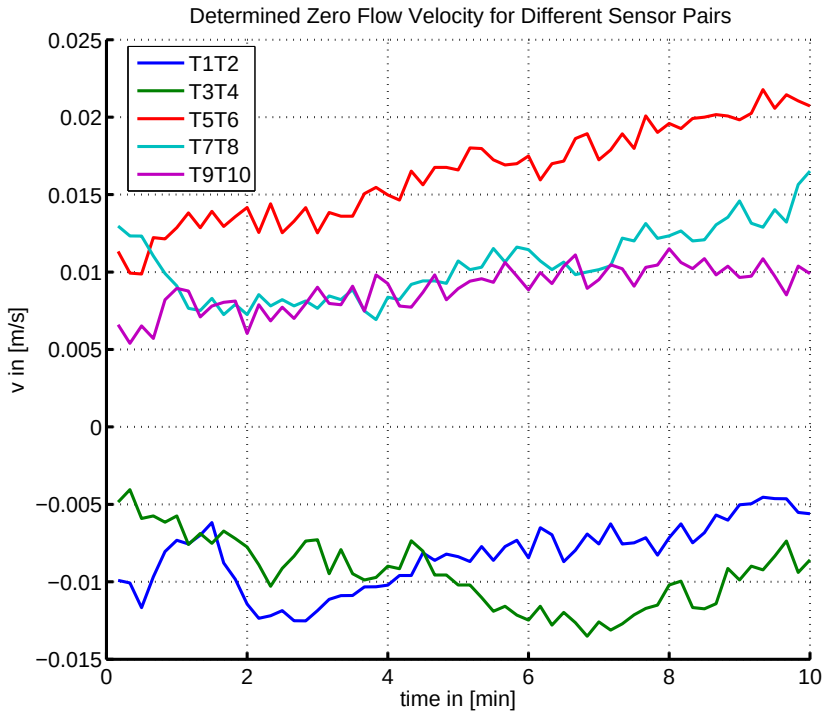


*Figure 3.8: Short term zero flow robustness for different sensor pairs*

ducer pairs. It is interesting to note the magnitude of the biases is around 1 cm for all five transducer pairs. In general the standard deviation is the most important measure to characterize the estimation process, because a constant bias in the estimation can be removed by calibration. This is not the case for transducer pair T9T10 where the bias is increasing over time.

Especially in the case of zero flow measurements the bias or accuracy is an import performance measure as well, because the reference flow is known to be zero. Theoretical simulations by AVL have shown however, that minimal fluctuations, i.e. convection, can occur, if a temperature gradient exists along the pipe, resulting in flow velocities as high as $\pm 1\frac{cm}{s}$. Another problem is the low-vibration storage of the measurement pipe.

To quantify the accuracy of the different measurements, the mean values are given in Tab. 3.4. Fig. 3.9 gives an example of the four different flow velocity estimates for transducer pair T7T8. Due to phase discontinuities $\hat{v}_{ref}$ (green) frequently jumps by $\sim 25\frac{cm}{s}$.

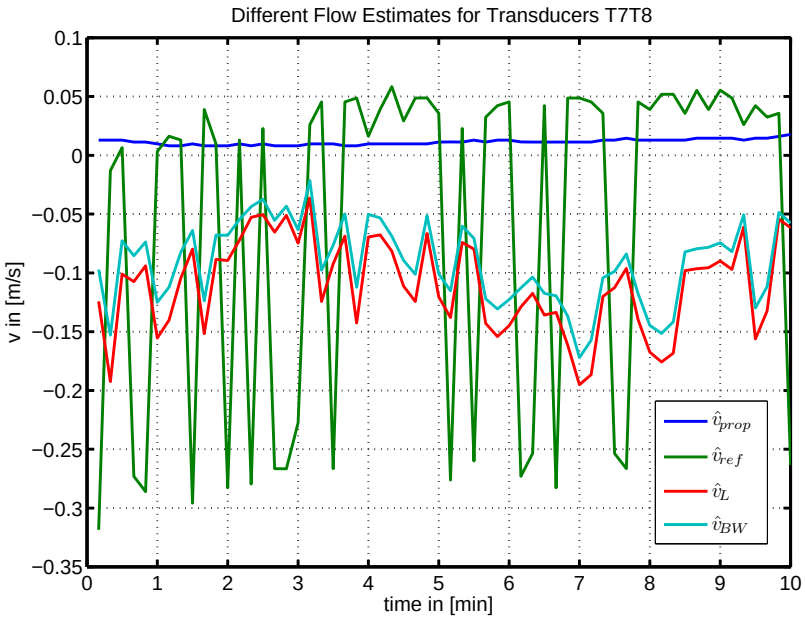


*Figure 3.9: Short term zero flow estimates for transducer pair T7T8*

| | T1T2 | T3T4 | T5T6 | T7T8 | T9T10 | RMS |
|---|---|---|---|---|---|---|
| mean of $\hat{v}_{ref}$ in [cm/s] | 3 | 0.5 | -7.1 | -5.6 | -9.6 | 6.1 |
| mean of $\hat{v}_L$ in [cm/s] | -0.9 | 8.6. | -9.1 | -11 | 2.7 | 7.56 |
| mean of $\hat{v}_{BW}$ in [cm/s] | -3.1 | 3.3 | -15.5 | -9.1 | 1.6 | 8.31 |
| mean of $\hat{v}_{prop}$ in [cm/s] | -0.8 | -0.9 | 1.7 | 1.1 | 1 | 1.14 |

*Table 3.4: Standard Deviation of Zero-Flow Measurement Results of Different Sensor Pairs*

The results in Tab. 3.4 have to be treated with caution since the averaging is only done over 60 measurements for each transducer pair. As in the example of Fig. 3.9, the mean of $\hat{v}_{ref}$ depends heavily on the number of jumps within the measurement period. To get a statistically reliable result longer measurements are needed.

However the results for the different flow estimation methods can still be compared. As for the precision in Tab. 3.3, the accuracy of the proposed method is best. It is interesting to see that the mean of $\hat{v}_{BW}$ is greater than the mean of $\hat{v}_L$. Even more surprising both are higher than the mean of the reference method. As stated above, the statistical significance of this result is however questionable due to the small number of measurements.

### 3.3.2 Long Term Measurement

In this section the results of a long term measurement are presented. Fig. 3.10 shows the estimated flow velocity for sensor pair 9&10 over 3 days, estimated with the reference method (red) and the proposed method(blue). Measurements were taken every ten minutes. The bias voltage was left unchanged to induce polarization and alter the transmission behavior of the transducers. The measurement was performed in an office. It was started at 5 p.m. on a Friday and stopped at 9 a.m. on a Monday to minimize vibrations by moving people.

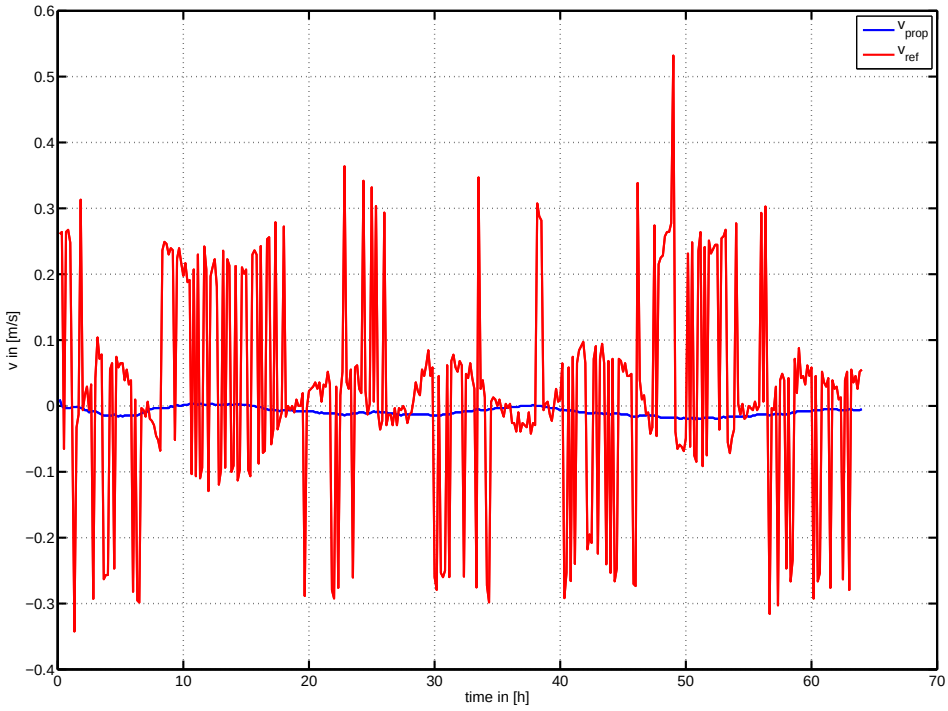


*Figure 3.10: Long term zero flow robustness - proposed method vs. reference method for Sensors 9&10*

The phase ambiguities as well as the drift effects, due to changes in the transducer parameters, lead to an error for the reference method in the range of $\pm 0.25 \frac{m}{s}$ which is in accordance with the results from the short term measurements. The proposed method gets rid of the phase ambiguities and reduces the drift effects to $\pm 0.01 \frac{m}{s}$, achieving the required precision.

Fig. 3.11 shows the transducer parameters over time, the upper 3 dB cut-off frequency (top line), the center frequency (middle line), and the lower 3 dB cut-off frequency. Judging from the development of the bandpass characteristics of the upstream (blue) and the downstream (red), it becomes evident that the assumption of reciprocity may not hold

under all circumstances. Especially betwen $t = 20\,h$ and $t = 30\,h$ the difference between upstream and downstream become apparent. These deviations are not random , as shown below.

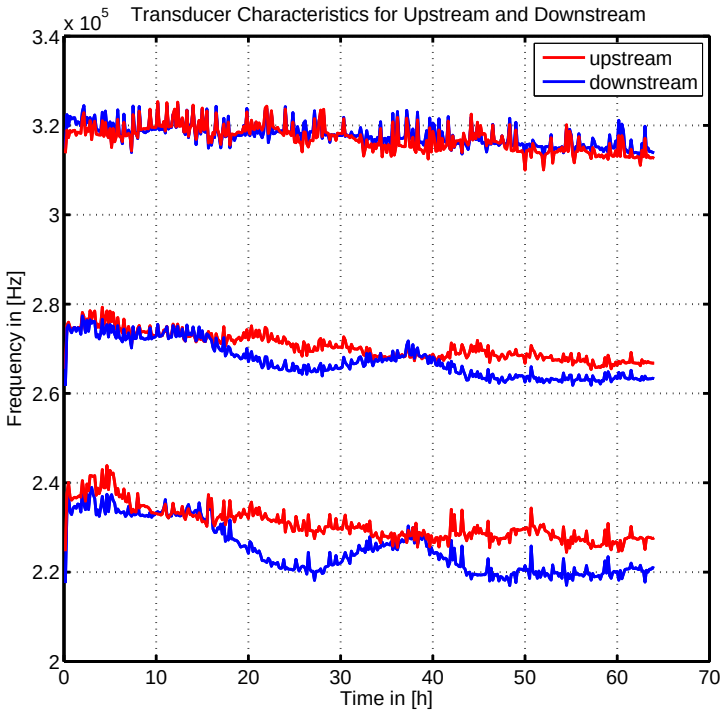


*Figure 3.11: Parameter drift of upstream and downstream identified systems for sensors 9&10*

Even though the center frequencies of the transmission system drop roughly 20 kHz and the bandwidth changes accordingly over the course of 3 days, the proposed method still estimates the flow velocity with the requested precision. As opposed to the short term measurements, the estimation errors of subsequent measurements are not independent. The variance of the error is therefore not directly comparable with the variances from Section 3.3.1, because for the long term measurement, the time varying bias is included in the variance.

What appears to be random ripple, especially in the trace of the upper 3 dB cut-off frequency is shown in detail in Fig. 3.12. The first idea that comes to mind, is that the estimation of the cut-off frequencies is simply affected by noise. This idea can be dismissed when looking at this figure. It can be seen that the deviations are not random, but they occur both in the upstream and downstream measurement. Taking into account the measurement interval of 10 minutes, the reason for this ripple could be changing transducer characteristics, or artefacts from the MLS based system identification..

Fig. 3.13 shows the reciprocity measures $\Delta_C$, $\Delta_B$ and $\Delta_G$ as introduced in Section 2.1.3, together with the proposed flow velocity estimate. At $t = 0$ a jump occurs due to a re-

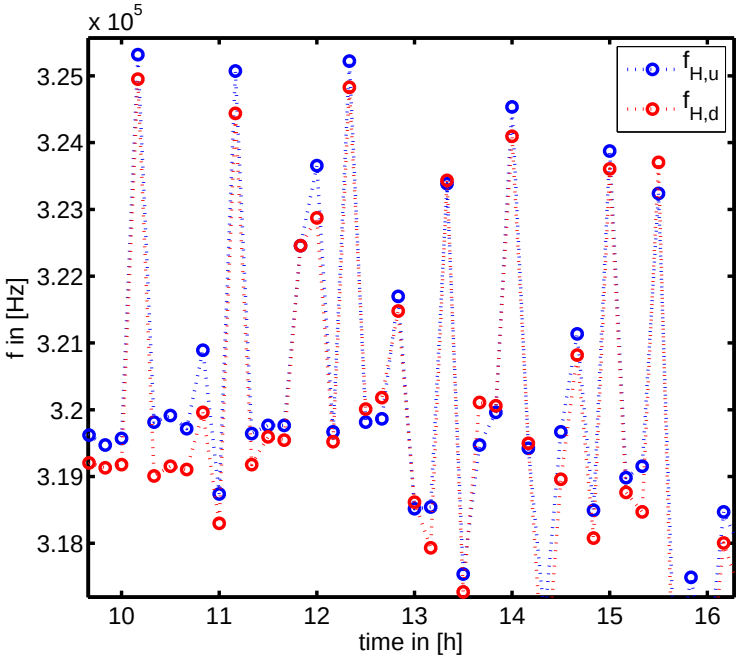


*Figure 3.12: Close-up of Fig. 3.11, upstream and downstream 3 dB cutoff frequencies $f_{H,u}$ and $f_{H,d}$*

adjustment of the bias voltage right after the beginning of the measurement. $\Delta_C$ and $\Delta_B$ are given as relative measures, i.e. divided by the average center frequency and bandwidth respectively. Since the average of the group delay would be zero, $\Delta_G$ is given as absolute value.

Fig. 3.14 shows the upstream (blue) and downstream (green) identified magnitude responses as well as the the division of the two magnitude responses (red), at the two exemplary time indices $t = 38\,h$ (high reciprocity) on the left side and $t = 50\,h$ (low reciprocity) on the right side. For ideal reciprocity the magnitude response of the division should equal a straight horizontal line at 0 dB. The difference in the identified magnitude responses is clearly greater in the case of non reciprocity (right side), which can also be seen from the magnitude of the division. Fig. 3.14 also shows that the 3 dB cut-off frequencies of upstream and downstream really differ, and that not only a ripple in the passband is responsible for the difference. It is not clear why this non reciprocity occurs.

It is evident that there is a strong correlation between the reciprocity measures and the flow velocity estimate. The regions where $\Delta_C$, $\Delta_B$ and $\Delta_G$ are small correspond to regions where the flow velocity is estimated correctly to be zero. This is in accordance with the observations made by [7, Deventer et al.] that non-reciprocity leads to bias in the estimation of the flow velocity. Since the reciprocity measures are heavily correlated with the accuracy of the flow velocity estimation, this knowledge can be used to extract the correlated amount of the estimation error from the flow velocity estimate (Section 3.3.3).

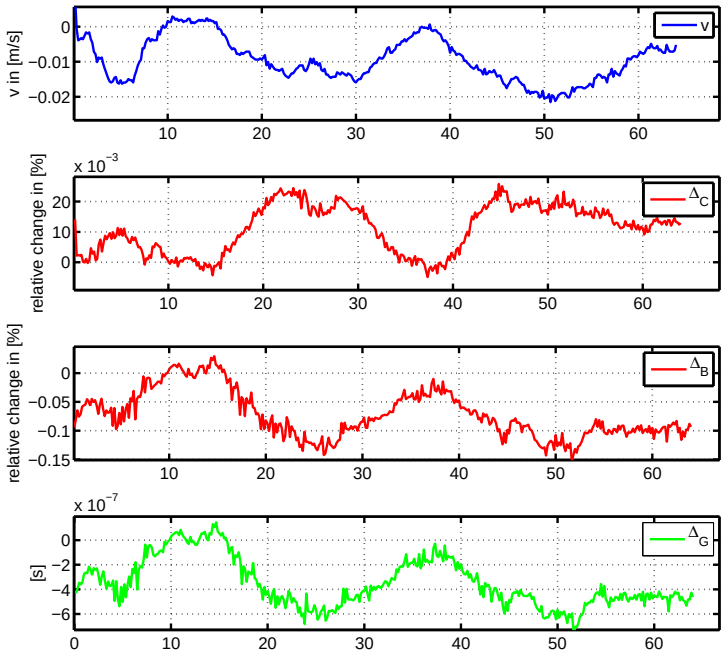


*Figure 3.13: Flow velocity $v$ vs. reciprocity measures $\Delta_B$, $\Delta_C$ and $\Delta_G$*

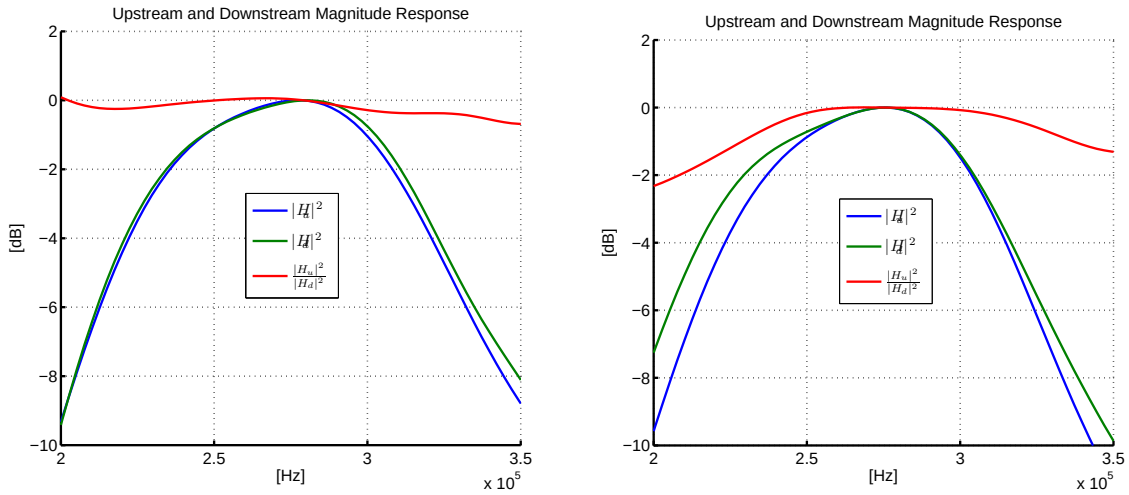


(a) High reciprocity at $t = 38h$

(b) Low reciprocity at $t = 50h$

*Figure 3.14: Magnitude responses of $H_u$, $H_d$ and $\frac{H_u}{H_d}$*

It is however uncertain if the dependence between the reciprocity measures and the flow velocity estimate is universally valid. E.g. it could depend on the transducer pair. At least in a post processing step, once all measurements have been made, the resulting flow velocity estimate can be checked for correlation with the reciprocity measures, and corrected accordingly.

For low flow velocities and constant temperatures, the deviations of the estimated flow velocity occur only due the variations of $\hat{\Delta}_t$. In the proposed method $\Delta_t$ is measured directly via the cross correlation method, so no additional information that is gained by system identification is used. As shown in Tab. 3.2 the direct computation is still significantly more precise than all other investigated methods. The varying reciprocity may be linked to the initial state of the transducers, i.e. if they are matched to have the same frequency response.

### 3.3.3 Post Processing with Reciprocity Measures

The correlation between the reciprocity measure $\Delta_B$ (difference of bandwith in upstream and downstream) and $\Delta_t$ can be used to remove bias in the flow velocity estimate. The left side of Fig. 3.15 shows the reciprocity measures $\Delta_B$ and $\Delta_G$ (group delay of $H_u/H_d$) for the long term measurement of Section 3.3.2. Both measures have been normalized to the same range to make them comparable, since the unit of $\Delta_B$ is frequency and the unit of $\Delta_G$ is seconds. Almost perfect correlation can be observed. It is convenient to use $\Delta_G$ because it already has the same unit as $\Delta_t$.

On the right side of Fig. 3.15, $\Delta_G$ is shown together with $\Delta_t$. The range of $\Delta_G$ is at least one order of magnitude higher than the range of $\Delta_t$.

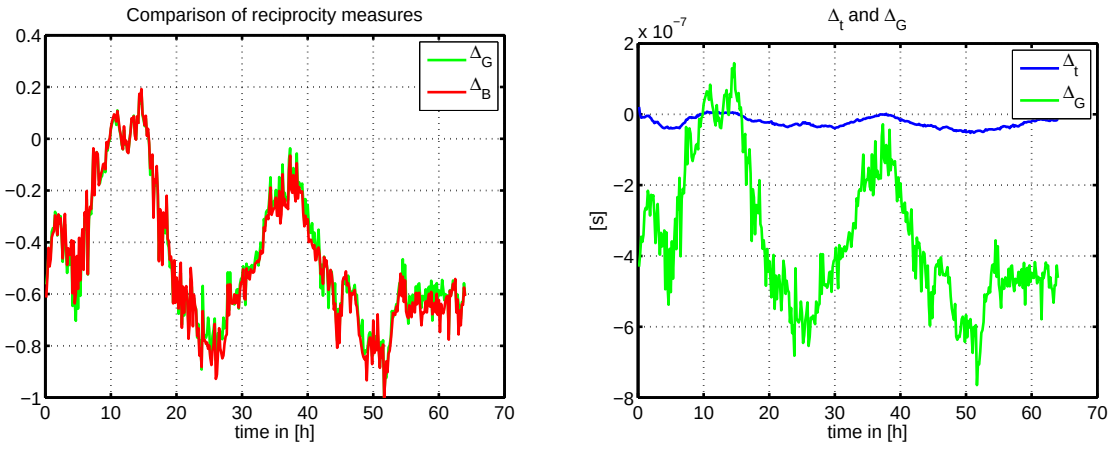


(a) Correlation of $\Delta_G$ and $\Delta_B$

(b) $\Delta_t$ vs. $\Delta_G$

*Figure 3.15: Correlation of reciprocity measures and $\Delta_t$*

Fig. 3.16 shows on the left, that there is a linear dependency between $\Delta_G$ and $\Delta_T$. This dependency is modeled by a 1st order polynomial (i.e. a straight line) $p(\Delta_G)$. The evaluation of the polynomial at the values of $\Delta_G$ is shown on the right side of Fig. 3.16 (green). The result is very similar to the estimated transit time difference. The magenta

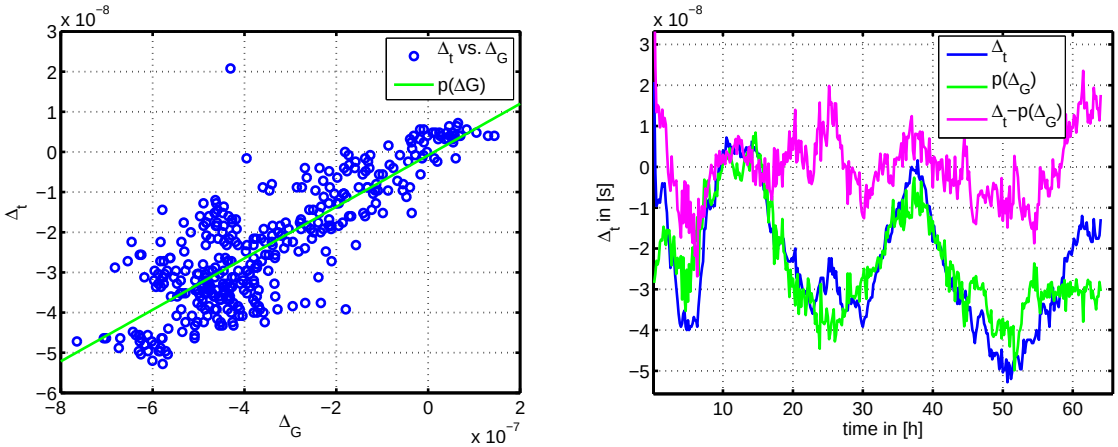


(a) Relation of $\Delta_G$ and $\Delta_t$ and line fitting

(b) Bias correction of $\Delta_t$

*Figure 3.16: Using correlation of $\Delta_t$ and $\Delta_G$ to improve estimation of $\Delta_t$*

graph is the estimated flow velocity, where the correlated part of $\Delta_G$ is subtracted. Using

$$\hat{v}_{prop,c} = \hat{v}_{prop} - p(\Delta_G) \tag{3.6}$$

Fig. 3.17 shows the result of the bias correction. On the left hand side the proposed flow velocity estimate $\hat{v}_{prop}$ is compared to the bias corrected estimate $\hat{v}_{prop,c}$. On the right hand side, the reference estimate $\hat{v}_{ref}$ is included. It can be seen that the bias can be significantly reduced. The accuracy of the resulting flow estimate is considerably higher after bias correction.

It is beyond the scope of this work to investigate the relationship between the reciprocity measure and the transit time difference estimate. There is great potential in exploiting this knowledge, to make a real-time bias correction possible.

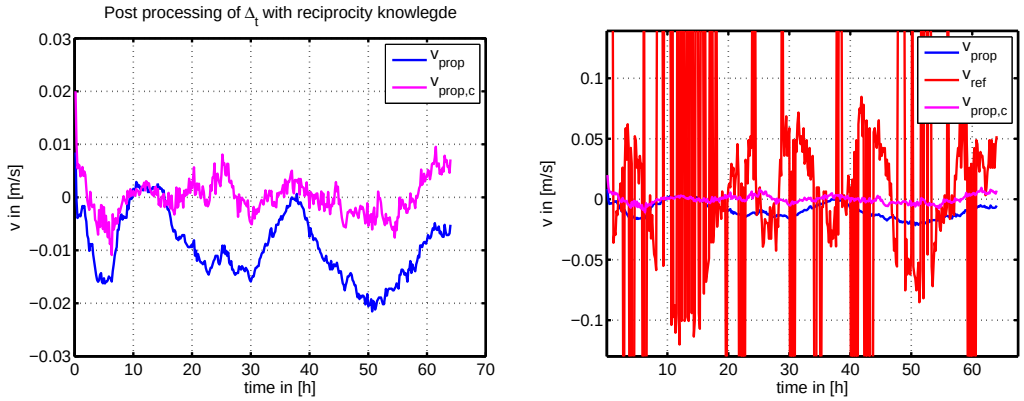


(a) Proposed flow velocity estimated with bias correction

(b) Comparison with reference method

*Figure 3.17: Bias correction of flow velocity estimate*

# 4 Conclusion

*"If you copy from one author, it's plagiarism. If you copy from two, it's research."*
*– Wilson Mizner*

After an introduction to transit time flowmetering, the theoretical background for system identification with $m$-sequences was explained. The required methods for the proposed algorithm have been described, especially group delay estimation and robust transit time estimation. Theoretical considerations regarding performance bounds have been made, and shown to help understanding the achievable precision.

The algorithm proposed in this thesis achieves the required absolute accuracy and precision of $\pm 1\ \frac{cm}{s}$. The knowledge of how to characterize the transducers, along with the idea of coherent phase measurement and the direct estimation of the transit time difference $\Delta_t$ are the most important steps that helped to achieve this goal.

Both short and longterm measurements show the advantage of the proposed method as opposed to traditional algorithms. In spite of an artificial parameter drift caused by polarization, long term stability can be achieved. The dependence on the parameter drift of the transducers has been reduced by perpetual system identification and subsequent band pass model fitting.

The variations in the estimated flow velocity have been shown to be correlated with the reciprocity of the transducers. The proposed algorithm is also applicable for other transit time measurement setups, including other measurement signals, transducer characteristics and geometries.

## 4.1 Future Work

Better understanding of the relationship and causality between reciprocity and the precision of the estimation of the transit time difference $\Delta_t$ is yet to be gained, since this knowledge is extremely helpful in correcting the estimation bias. Flow measurements with reference flows and under different environmental conditions (i.e. temperature, pressure, transducer mountings, etc...) should be performed to validate the proposed algorithm.

The bandpass model fitting with a butterworth filter does not allow for different gains of the two transducer models. The least squares method can account for different gain factors, at the cost of occasionally resulting in an unstable bandpass model. A compromise between the two methods, could be beneficial.

Experiments with different signals and pulse shapes to improve the measurement precision of $\Delta_t$ could improve even more the robustness for measurements at low flow velocities, if the cross correlation properties of the signals are considered. Averaging the upstream and downstream identified system and using only one model for group delay correction could be beneficial in terms of robustness. Also the information of the actual reciprocity should be used to reduce the estimation variance.

Measurement setups under real conditions should give insight into the rate of change of the transducer parameter drift. With this knowledge the system identification could be performed less often, making use of other signals in the meantime possible.

# Bibliography

[1] M. Wiesinger, "Entwicklung eines Abgas-Massenflusssensors," Ph.D. dissertation, TU Wien, 1999.

[2] M. Kupnik, "Ultrasonic transit-time gas flowmeter for automotive applications," Ph.D. dissertation, University of Leoben, 2004.

[3] L. Lynnworth and Y. Liu, "Ultrasonic flowmeters: Half-century progress report, 1955-2005," *Ultrasonics*, vol. 44, Supplement, pp. 1371–1378, 2006.

[4] S. Jacobson, "New developments in ultrasonic gas analysis and flowmetering," in *Ultrasonics Symposium, 2008. IUS 2008. IEEE*, 2008.

[5] P. D. Lysak, D. M. Jenkins, D. E. Capone, and W. L. Brown, "Analytical model of an ultrasonic cross-correlation flow meter, part 1: Stochastic modeling of turbulence," *Flow Measurement and Instrumentation*, vol. 19, pp. 1 – 7, 2008.

[6] ——, "Analytical model of an ultrasonic cross-correlation flow meter, part 2: Application," *Flow Measurement and Instrumentation*, vol. 19, no. 1, pp. 41 – 46, 2008.

[7] J. van Deventer and J. Delsing, "Apparent transducer non-reciprocity in an ultrasonic flow meter," *Ultrasonics*, vol. 40, pp. 403 – 405, 2002.

[8] A. Caronti, G. Caliano, A. Iula, and M. Pappalardo, "An accurate model for capacitive micromachined ultrasonic transducers," *Ultrasonics, Ferroelectrics and Frequency Control, IEEE Transactions on*, vol. 49, pp. 159 –168, 2002.

[9] J. Berrebi, J. van Deventer, and J. Delsing, "Reducing the flow measurement error caused by pulsations in flows," *Flow Measurement and Instrumentation*, vol. 15, pp. 311 – 315, 2004.

[10] W.T. and Chu, "Impulse-response and reverberation-decay measurements made by using a periodic pseudorandom sequence," *Applied Acoustics*, vol. 29, pp. 193 – 205, 1990.

[11] N. Xiang, "Using m-sequences for determining the impulse responses of lti-systems," *Signal Processing*, vol. 28, pp. 139 – 152, 1992.

[12] A. V. Oppenheim and R. W. Schafer, *Discrete-time signal processing.* Upper Saddle River, NJ, USA: Prentice-Hall, Inc., 1989.

[13] M. J. Anderson and X. Liu, "Use of reciprocity to characterize ultrasonic transducers in air above 100 khz," *JASA*, vol. 103, pp. 446–453, 1998.

[14] S. M. Kay, *Fundamentals of Statistical Signal Processing - Estimation Theory.* Prentice-Hall, Inc., 1993.

[15] U. Tietze and C. Schenk, *Halbleiter-Schaltungstechnik*, 10th ed. Springer-Verlag, 1993.